A multi-technique dating study of two Lower Palaeolithic sites from the Cher valley (Middle Loire Catchment, France): Lunery-la Terre-des-Sablons and Brinay-la Noira

Mathieu Duval[1,2], Pierre Voinchet[3], Lee J. Arnold[4], Josep M. Parés[2], Walter Minnella[5], Verónica Guilarte[6], Martina Demuro[4], Christophe Falguères[3], Jean-Jacques Bahain[3] & Jackie Despriée[3]

[1] Australian Research Centre for Human Evolution (ARCHE), Environmental futures Research Institute, Griffith University, NATHAN QLD 4111, Australia. E-mail: m.duval@griffith.edu.au

[2] Geochronology and Geology, Centro Nacional de Investigación sobre la Evolución Humana, Paseo de Atapuerca, 3, 09002 Burgos, Spain

[3] UMR 7194 HNHP, Museum National d'Histoire Naturelle, Département Homme et environnement, 1 rue René Panhard, 75013 PARIS.

[4] School of Physical Sciences, Institute for Photonics and Advanced Sensing (IPAS) and Environment Institute, University of Adelaide, North Terrace Campus, ADELAIDE, SA 5005, Australia

[5] PH3DRA Laboratories (PHysics for Dating Diagnostic Dosimetry Research and Applications), Dipartimento di Fisica e Astronomia, Università di Catania & INFN – Catania, Via Santa Sofia 64, 95123 Catania, Italy

[6] Departamento de Didáctica de las Ciencias Experimentales. Facultad de Educación y Humanidades de Melilla. Universidad de Granada, Spain.

Abstract

We present the results of a new dating study carried out at Lunery-la Terre-des-Sablons (LTS) and Brinay-la Noira (BN), two key Lower Palaeolithic sites located in deposits associated to the Cher River (Middle Loire Catchment, France). These sites preserve abundant Mode 1 and Mode 2 lithic industries, and are considered as among the oldest evidence of hominin presence in Western Europe north of the 45°N latitude. Following a multi-technique approach combining electron spin resonance (ESR), single-grain thermally-transferred optically stimulated luminescence (TT-OSL) dating of quartz grains and palaeomagnetism, we obtain new chronological constraints for the sedimentary sequence, and the associated lithic assemblages, at the two sites.

The new independent dating results derived from each method are consistent and in overall agreement with existing ESR and terrestrial cosmogenic nuclide (TCN) age estimates, except for the Lowermost Unit 3 at LTS. By integrating all of the previous and new dating results, we derive combined age estimates of 772-735 ka and 665 ± 29 ka for the fluvial sands at LTS (Unit 1) and BN, respectively. These two distinct aggradation phases may tentatively be correlated to interglacial/glacial transitions associated with Marine Isotope Stage (MIS) 19-18 for the former and MIS 17-16 for the latter.

At BN, an age range of 638-676 ka may be proposed for the hominin occupation after combining numerical age results and geological evidence. This result is consistent with the initial chronology proposed by Moncel et al (2013) [Moncel, M.H., Despriée, J., Voinchet, P., Tissoux, H., Moreno, D., Bahain, J. J., Courcimault, G., Falgueres, C. (2013). Early evidence of Acheulean settlement in north-western Europe – la Noira site, a 700 000 year-old occupation in the Centre of France. Plos One, 8(11): 1-22] and confirms that BN is among the oldest Acheulean occurrences in Western Europe.

At LTS, the mean age of 710 ± 50 ka obtained for the sandy layer in Unit 3 provides a minimum age constraint for the archaeological level located below. The major sedimentary disconformity observed between the fluvial deposits and the underlying pebble layers hosting the lithic artefacts suggests that the true age of the artefacts might be significantly older, probably Early Pleistocene given their similarities with other Mode 1 assemblages identified in Western Europe. However, further refinement of the Mode 1 chronological inference at LTS remains difficult at this stage.

Finally, these new dating results show the importance of using the Multiple Centre approach for ESR dating of quartz grains, and confirm the value of combining different dating methods in order to build more robust chronologies for Lower Palaeolithic sites in Europe.

From a methodological point of view, the dating results presented here are especially encouraging for the reliability of the ESR method applied to optically bleached quartz grains. This is one of the very first studies demonstrating that samples independently dated by two different laboratories may produce generally reproducible ESR age results.

Introduction

Over the last three decades, the Quaternary fluvial deposits of the Loire catchment and its tributaries (France) have been extensively and systematically studied from a multidisciplinary perspective. This long-term investigation initiated by a team of researchers from the Muséum National d'Histoire Naturelle (MNHN) in Paris, France, has led to the identification of different stepped terrace systems for the Loir, Cher and Creuse valleys (see an overview in Voinchet et al., 2010 and Depriée et al., 2011). The deposits have been chronologically constrained by an unprecedented large number of Electron Spin Resonance (ESR) ages (n>200) based on optically bleached quartz grains. Most of the work has been focused on the measurement of the aluminium (Al) centre (e.g. Voinchet, 2002; Voinchet et al., 2010; Despriée et al., 2011; Garon et al., 2017), although a few attempts at dating the titanium (Ti) centres have also been reported (Tissoux et al., 2007). These dating results have established a robust and detailed regional chronostratigraphic framework for the fluvial deposits covering most of the Pleistocene. Additionally, a systematic archaeological survey of the fluvial terraces has led to the identification of several tens of localities with Palaeolithic assemblages, some of which are amongst the oldest evidence of hominin presence in Western Europe (e.g. Despriée et al., 2006, 2011, Moncel et al., 2013). In particular, two localities are of major interest in the Cher valley (Middle Loire catchment): Lunery-la Terre-des-Sablons and Brinay-la Noira. The first of these sites has provided Mode 1 (or Oldowan, depending on the terminology employed; Carbonell et al., 2015) lithic artefacts dated to between 0.9 and 1.1-1.2 million years ago (Ma) (Despriée et al., 2017a), while the latter has yielded a Mode 2 (or Acheulean) assemblage dated to 600-700 ka (Moncel et al., 2013). The chronology of each site has been constrained by ESR ages from several samples collected throughout the sequences. These results are internally consistent and stratigraphically coherent at a given site, producing an apparently robust chronostratigraphic framework. That said, unequivocal independent age control is absent from these sites. The only reported attempt so far has been made with terrestrial cosmogenic nuclide (TCN) burial dating, which led to somewhat inconclusive results according to the authors (Shen et al., 2012). For a long time, cross-comparisons have been almost impossible, as the geological context and reported age of these sites has strongly limited the use of other dating methods. For example, there is no suitable material for U-series or Ar-Ar dating applications. Moreover, the absence of fossils at these sites precludes not only any biochronological inference but also the use of the ESR method applied to teeth. Additionally, the limited thickness of the sedimentary sequences and the predominantly unconsolidated coarse sand deposits are not ideally suited for a proper and detailed magnetostratigraphic study. Finally, the dose saturation limitation of conventional optically stimulated luminescence (OSL) signals has typically restricted the applicability of this sediment dating method to late Middle to Late Pleistocene deposits, i.e. much younger than the published age of the two sites.

However, methodological advances over the past two decades have expanded the applicability of dating techniques and improved their reliability. In particular, new extended-range luminescence dating techniques such as single-grain thermally transferred OSL (TT-OSL) have provided reliable age estimates for Early Pleistocene deposits (e.g., Arnold et al., 2015; Bartz et al., 2018). Since the publication of the ESR ages at Lunery-la Terre-des-Sablons and Brinay-la Noira, there have also been a number of significant methodological developments in the ESR dating approach for optically bleached quartz grains. Among them, the exponential+linear (EXP+LIN) function was recently found to be more appropriate than the Single Saturating Exponential (SSE) function for fitting the ESR intensities of the Al centre (Duval, 2012; Voinchet et al., 2013). The most significant recent breakthrough is undoubtedly the increasing use of the Multiple Centre (MC) approach in ESR dating application studies. First proposed by Toyoda et al. (2000), it has progressively become a standard requirement in the field of ESR dating of optically quartz grains (e.g. Duval et al., 2017a; Pereira et al., 2018). Based on the systematic measurement of both the Al and Ti centres in a given quartz sample, it is considered as the best way to evaluate the inherent uncertainty associated with possible incomplete resetting of the Al signal prior to sediment deposition (see an overview in section 2 of Duval et al., 2017a).

In light of these recent advancements, a series of new ESR samples was collected in April 2011 at Brinay-la Noira and Lunery-la Terre-des-Sablons sites (Cher department) with the aim of re-examining and refining the existing ESR chronologies of the sites. The new samples were processed at the Centro Nacional de Investigación sobre la Evolución Humana (CENIEH) following the standard MC procedure described in Duval et al. (2017), i.e. in a completely independent way to those produced earlier by the MNHN research team for the same sites. Additional samples were also collected for extended-range luminescence dating and palaeomagnetic analyses in order to obtain independent age control and evaluate the accuracy of the ESR results.

In summary, the present multi-technique dating study aims not only at evaluating the reproducibility and accuracy of the ESR dating method applied to optically bleached quartz grains, but also at further constraining the chronology of two key Lower Palaeolithic localities located north of the 45°N latitude. The general implications of the refined chronologies will also be discussed, and in particular regarding the stratigraphic interpretation of the sites.

Finally, because ESR, Luminescence and TCN age uncertainties are typically reported at a 1-σ confidence level (e.g. Duller, 2008; Duval et al., 2017b; Carbonell et al., 2008; Arnold et al., 2015), this common practice will apply here as well: all numerical ages mentioned in the present manuscript will be given with their corresponding 1-σ errors, unless mentioned otherwise.

1. Study area

1.1. The Cher valley

A total of nine stepped terraces have been identified and extensively dated by ESR in the Cher valley over ~50 m of vertical incision (Fig. 1). Named sequentially from A (current floodplain deposits) to I (+45 m above the bedrock floor of A), these terraces have chronologies covering the last ~1.3 Ma (Voinchet et al., 2010). Archaeological surveys of those deposits has led to the discovery of several Palaeolithic sites with lithic artefacts attributed to different techno-complexes and found in primary position (i.e., not reworked; see a detailed overview in Despriée et al., 2011). The oldest artefacts, characterised as Mode 1 assemblages, were found in stacked terraces F (+28-34 m) and G (+34-40 m) at the same locality of Lunery-la-Terre-des-Sablons, and have been dated to about 0.9 and 1.1-1.2 Ma, respectively (see further detail in section 1.2.). Mode 2 assemblages have been documented at Brinay-la Noira, Gièvres-la-Genetière and Gièvres-la-Plaine-de-la-Morandière localities (Loir-et-Cher department), all correlated to fluvial terrace D (+14-21 m) and dated to about 650 ka (see Despriée et al., 2011 and references therein). Finally, a lithic assemblage with more advanced features (Levallois debitage) has also been reported in Terrace B (+5-11 m) at Gièvres-la Morandière (Loir-et-Cher department), and dated to around 370 ka (Fig. 1). Together, these occurrences indicate the recurrent presence of hominins in the area since the latest part of the Early Pleistocene.

Figure 1 approx. here

1.2. Lunery-la Terre-des-sablons (LTS)

The LTS locality corresponds to a former sand quarry, a few km north of the village of Lunery. Stratigraphic interpretation of the site based on sedimentological and chronological evidence combined with field observations have led to the identification of three superimposed sandy units (labelled 1 to 3 from top to bottom) deposited on the Oxfordian limestone bedrock, which has been identified at different depths across the site (Fig. 2). These units are preserved on a tilted main block (called "*les Sablons"* block) bordered on the western edge by the so-called Rosières fault and by the Cher river in the East. Successive fault reactivations until the Pleistocene have broken the Jurassic limestone in long and narrow smaller blocks. The course of the Cher river is presently flowing about 1 km east from the site (further details about the geological context may be found in Despriée et al., 2007, 2017a and Voinchet et al., 2007).

Figure 2 approx. here

Presently, the coarse red sandy Unit 3 is deposited on the lower block (-12m below the top of the sequence; Fig.3), while the beige sandy Unit 2 is deposited on the middle block (-9 m), both with a similar horizontal extension of about 50 m. The sandy Unit 1 is deposited on the highest limestone floor (-5m) over a 500-m width and covers both units 3 and 2 (Despriée et al., 2017a; Fig. 2). The current relative altitude of Unit 1 is +29-34 m, but geological evidence suggest that this altitude may have been somewhat higher in the past, i.e. before the les Sablons block was downthrown, probably concomitant with the overstretching of the Cher graben (Despriée et al, 2017c). Similarly, the older Units 2 and 3 that are now covered by Unit 1 were most likely originally deposited at this relative altitude or possibly even higher. The absence of others sedimentary remnants from these two units suggests that they were probably deposited higher on the previously eroded western slope (see further details in Despriée et al., 2017a).

Unit 3 is about 2.20 m thick and lies on top of the Oxfordian limestone located about 12 m below the surface. The bottom part of the lower layer (*a*) consists of ca. 30 cm of periglacial diamicton containing blocks, cobbles and pebbles of materials derived from Neogene river deposits from the plateau and the slope, and mixed with clayey sand and iron pisoliths. This deposit is cryoturbated, with polygons and clusters of cobbles (Despriée et al., 2017a). A Mode 1 lithic assemblage (> 700 artefacts) divided into three archaeological horizons has been identified within the basal diamicton of layer a. The raw materials used are Jurassic oolitic silicifications and lacustrine millstone slabs. There is no evidence of transport on the artefacts, suggesting that they were found in primary position (Despriée et al., 2010a and b). The diamicton is overlain by a 20 cm-thick bed of locally derived pebbles and small cobbles with structures that suggest deposition by slope wash processes. Finally, layer *b* above is made of 1.70 m-thick cross-bedded sands. Full details about the stratigraphy and site formation processes may be found in Despriée et al., 2017a (in particular see Figure 27 of Despriée et al., 2017a).

The three sediment samples collected from the fluvial deposits of layer b have provided consistent ESR results (Al centre) of 1102 ± 119, 1174 ± 122 and 1227 ± 123 ka (Despriée et al., 2017a; Detailed numerical results may be found in Supplementary Material, Table S1). The derived weighted mean age of 1166 ± 140 ka may be interpreted as a minimum age constraint for the lithic artefacts found stratigraphically below in layer *a*. These existing dating results mean that LTS preserves one of the oldest evidence of hominin presence in Europe, with a chronology similar to that of Fuente Nueva 3 (Duval et al., 2012) and Atapuerca Sima del Elefante TE9 (Carbonell et al., 2008). Finally, ^{26}Al/^{10}Be burial dating has also been performed on one quartz sand sample from layer *b* of Unit 3, about 11 m below the surface (Shen et al., 2012) and at the same stratigraphic position as the MNHN ESR samples. Assuming post-burial nuclide production or the absence of post-burial nuclide production resulted in very close estimates of 750 ± 240 and 710 ± 210 ka, respectively, which are younger than the corresponding ESR ages. The large uncertainties associated with the TCN age estimates arise from the high natural Al content of the sediments (>100 ppm), which led the authors to consider their results as preliminary.

Unit 2 is preserved over a maximum thickness of about 4.5m and comprises two coarse sand layers (*a* and *b*) (Fig. 3) positioned on top of the Oxfordian limestone located about 10 m deep below surface. Mode 1 lithic artefacts (mostly cores and choppers) were found at the base of layer *a* (Despriée et al., 2010, 2011). ESR dating of two samples (Al centre) from the middle of layer *b* have provided consistent age results of 936 ± 49 ka and 949 ± 94 ka (Despriée et al., 2017a; Table S1). The derived weighted mean age of 939 ± 85 ka may be interpreted as a minimum age constraint for the lithic artefacts of Unit 2 (Fig. 3).

Figure 3 approx. here

Finally, Unit 1 has a thickness of 5.5 m and comprises two reddish layers (*a* and *b*) of indurated coarse sands in a clay matrix (Fig. 3). Layer *a* lies on top of clays derived from the weathering of the limestone bedrock. ESR dating yielded two consistent results of 808 ± 71 and 839 ± 79 ka for layers *a* and *b*, respectively (Despriée et al, 2017a; Table S1). A third sample collected from the same unit but at another section located a few hundred meters from the site has provided a very similar result (831 ± 103 ka).

In summary, the sand layers of the three units identified at different relative altitudes show different sedimentary facies and also yield different depositional ages. This evidence suggests that the LTS Units are not coeval, but rather correspond to different aggradation events. Based on the existing dating results, Units 1, 2 and 3, have been tentatively correlated to fluvial terraces E, F and G of the general chronostratigraphic framework of the Cher Valley, respectively, while more recent tectonic events have significantly affected the original geometry and morphology of the deposits (Despriée et al., 2007, 2011, 2017a and b).

1.3.Brinay-la Noira (BN)

The 6-m thick sedimentary sequence at BN is correlated with fluvial terrace D (+14-21 m) of the Cher valley. It lies on top of an Upper Eocene-Oligocene lacustrine limestone and greenish clay (so-called "Calcaires et Argiles lacustres du Berry" formation). Four different layers have been locally identified above the bedrock, named *a* to *d* from bottom to top (Despriée, et al., 2017b; Fig. 4). Layer *a*, whose thickness laterally varies between 30-90 cm, is made of a very coarse sandy and clayey deposit, including numerous endogeneous pebbles, jurassic silicifications and millstone slabs in the lower part of the layer (sub-layer *a1*). The upper part (sub-layer *a2*) is interpreted as slope deposits. Above, layer *b* is composed of about 5 m of fluvial coarse sands that get finer to the top, and is covered by layer *c*, which comprises fine and middle-sized gravel deposits with many iron pisoliths, millstone slabs and well-rounded quartz pebbles. On top, layer *d* is a sandy brown silt layer including millstone debris with orange patina that may locally reach a thickness of 70 cm.

Figure 4 approx. here

Lithic artefacts (n = 630) were found *in situ* within layer *a1* during fieldwork and excavations performed between 2003 and 2014. The assemblage is dominated by large cutting tools, cores and flakes, and crude core-tools, mostly made from millstone slabs (90%), which overall conforms well with other early Acheulean sites in Europe (Moncel et al., 2013, 2018). Stratigraphic and sedimentological evidence suggest that the upper part of the slope deposits (layer a2) is somewhat younger than the lithic assemblage and accumulation of blocks and stones at the base of layer a (Despriée et al., 2011).

Six ESR sediment samples have been dated from the fluvial sands of layer *b*. The measurement of the Al centre provided consistent ages between 600-700 ka (Moncel et al., 2013; Table S2). Consequently, a weighted mean age of 665 ± 55 ka was derived for this unit, which may be interpreted as a minimum estimate for the underlying lithic assemblage located within layer *a*. These results make Brinay-la Noira one of the oldest Acheulean site in Europe (Moncel et al., 2018).

Three additional, unpublished, ESR dating results derived from the same analytical procedure as in Moncel et al. (2013) (see details in Table S2) provide additional chronological constraints at the top and base of the sedimentary sequence. One sample collected from layer *c* gave a maximum age of 448 ± 46 ka for the upper part of the sequence (note that this age has been briefly mentioned in Iovita et al., 2017, but no further details were provided). Although this age is stratigraphically consistent with the others from layer *b* located below, it is nevertheless suspected to be underestimated on stratigraphic grounds. The identification in the stratigraphic sequence of a continuous and horizontal bed of gravel at the base of layer *c* intersected by several ice wedges (Despriée et al, 2017b) indicates the presence of a palaeosurface probably created by erosion and short movements of sediments on the slope. Runoff waters have most likely removed most of the fine alluvium and concentrated the gravel. Consequently, the sands extracted from this level and dated by ESR were most likely, at least in part, reworked and exposed to sunlight during this erosion process, inducing some resetting of the signals. Two additional samples extracted from the upper (*a2*) and lower (*a1*) parts of layer *a* have provided ages of 645 ± 30 and 1090 ± 61 ka, respectively. The first of these ages is very close to those obtained from layer *b*, whereas the second age is significantly older than the published ESR dataset for layer *b*. This age discrepancy could be due to either incomplete resetting of the Al signal (as suggested by the different bleaching coefficients measured; Table S2) or contamination of the quartz samples by another population of older grains. Indeed, the lowermost sample was collected from slope deposits next to the accumulation of millstone plates and blocks. This very poorly sorted heterometric sand and gravel sediment most likely experienced little or even no river transport, which did not lead to a complete resetting of the ESR signal in quartz grains.

Finally, $^{26}Al/^{10}Be$ burial dating was performed on one quartz sand sample from layer *a* (Shen et al., 2012). Assuming either post-burial nuclide production or the absence of post-burial nuclide production resulted in very close estimates of 730 ± 210 ka and 700 ± 200 ka, respectively. Again, this sample exhibits large associated dating uncertainties due to the same reason detailed earlier for LTS. These preliminary TCN results are consistent with the ESR chronology available at this site.

2. Sampling

Bulk sediment samples were collected by hammering a thick PVC tube into the section in order to avoid exposure to sunlight. Two ESR samples were collected at LTS (Fig. S1): one (LUN1103) from the upper Unit 1 and another (LUN1101) at the bottom of the sequence within Unit 3. Unit 2 was not sampled due to the absence of accessible outcrop in 2011. Two samples were also taken at BN (Fig. S2), one (NOI1101) at the top of layer *b* and the second (NOI1104) from within layer *a* at the bottom of the local sequence. *In situ* measurement of the gamma dose rate was systematically performed for each sample at the exact same sampling spot with a NaI probe connected to an Inspector-1000 multichannel analyser. Additional raw sediment samples were also collected for laboratory analyses.

In parallel, samples were collected for single-grain TT-OSL dating and palaeomagnetic analyses at the same two localities. TT-OSL sample collection and *in situ* dosimetry assessments followed the procedures outlined in Demuro et al (2015). At LTS, TT-OSL sample CRF11-2 was collected within Unit 3, ~8 m to the left of LUN1101 (Fig. S1 C). At BN, TT-OSL sample CRF11-4 was taken from layer *a*, ~40 cm to the left of ESR sample NOI1104 (Fig. S2).

Sampling for palaeomagnetic analyses was challenging at the two sites: the deposits are dominated by unconsolidated coarse-grained sands, which precludes a proper high-resolution magnetostratigraphic study of the sequences. Whenever possible, fine-grained sandstones or siltstone layers were selected for sampling. These samples were obtained by cutting small cubes from oriented blocks (ca 300 cc) using a small ceramic knife. Because of their friability, block samples were often impregnated in the field with a 1:1 sodium silicate solution for magnetic analysis. At LTS, we sampled two locations within Units 1 and 3 (LUN1 and LUN2; Fig. 3 & Fig. S1), from which several subsamples were collected and analysed in the laboratory. At BN, we sampled three different horizons (Fig. 4). Samples NOR1-1 and NOR1-2 came from the archaeological layer and consist of clayish sandstones. Samples NOR1-3, 4 and 5 were collected from within the upper part of layer *a*. Lastly, sampling site NOR1-6 is located slightly north of the previous site and corresponds to a thin (4 cm) clayish layer within *b*.

3. Methods

3.1. ESR dating

Sediment samples were prepared in the laboratory under conditions of limited illumination following the standard procedure at CENIEH (e.g. Duval et al., 2017a). The 100-200 µm size fraction was collected after wet sieving. HCl (36%) was used to dissolve carbonates and H_2O_2 (30%) to eliminate organic matter. Heavy minerals and feldspars were removed with Sodium Polytungstate solutions having a density of rho (ρ) =2.72 and 2.62 g/ml, respectively. Then, magnetic minerals were eliminated using Neodymium magnets. The resulting samples were treated with HF (40%) for 40 minutes to eliminate the remaining feldspars and to etch quartz grains. Finally, HCl (18%) was added in order to remove any soluble fluoride.

Quartz grains were dated by using the standard Multiple Aliquots Additive Dose (MAAD) method. Each natural sample was divided into 14 multi-grain aliquots. Twelve aliquots for each sample were irradiated using a ^{137}Cs Gammacell-1000 source (dose rate = 7.3 Gy/min, relative 1σ-uncertainty = 2.3%) to the following doses: 199, 398, 597, 995, 1492, 2487, 4974, 7959, 11938, 19896, 29844 and 49640 Gy. One aliquot was kept unirradiated (natural aliquot), while the last aliquot was exposed to a SOL2 (Dr Hönle) solar light simulator for about 1240 h, in order to evaluate the non-bleachable residual ESR signals of the Al centre.

ESR measurements were carried out at CENIEH (Burgos, Spain), with an EMXmicro 6/1Bruker X-band ESR spectrometer coupled to a standard rectangular ER 4102ST cavity. To ensure constant experimental conditions over time, the temperature of the water circulating in the magnet is controlled and stabilized at 18 ºC by a water-cooled Thermo Scientific NESLAB ThermoFlex 3500 chiller, and the temperature of the room is kept constant at 20 ºC by an air conditioning unit. ESR measurements were performed at low temperature (~90 K) using a ER4141VT Digital Temperature control system based on liquid nitrogen cooling. Further details about the setup and about its stability over time can be found in Duval and Guilarte Moreno (2012).

In accordance with the Multiple Centre method defined by Toyoda et al. (2000), the ESR signals of both the Al and Ti centres were measured. For the Al centre, the following acquisition parameters were used: 10 mW microwave power, 1024 points resolution, 20 mT sweep width, 100 kHz modulation frequency, 0.1 mT modulation amplitude, 40 ms conversion time, 10 ms time constant and 1 scan. In contrast, the ESR signal associated with Ti centres was measured as follows: 5 mW microwave power, 1024 points resolution, 20 mT sweep width, 100 kHz modulation frequency, 0.1 mT modulation amplitude, 60 ms conversion time, 10 ms time constant and 2 to 4 scans (depending on the aliquot). Each of the 14 aliquots of a given sample were measured 3 times after a ~120° rotation in the cavity for both Al and Ti signals in order to consider angular dependence of the signal due to sample heterogeneity. All measurements were repeated three times over distinct days in order to check the repeatability of the D_E values

(Tables 1 & 2). Consequently, three sets of 14 data points were obtained for each signal measured (Ti and Al) in a given quartz sample.

The ESR intensity of the Al signal was extracted from peak-to-peak amplitude measurements between the top of the first peak (g=2.0185) and the bottom of the 16th peak (g=1.9928) (Toyoda and Falguères, 2003). The ESR intensity of the Ti centres was measured as in Duval and Guilarte (2015): peak-to-peak amplitude between g=1.979 and g=1.913 (option A), peak-to-baseline amplitude around g=1.915 (Ti-H, Option C), peak-to-baseline amplitude around g=1.913-1.915 (option D), and peak-to-baseline amplitude around g=1.979 (option E).

For each aliquot, ESR intensities of Al and Ti centres were corrected by the corresponding receiver gain value, number of scans, mass and a temperature correction factor (Duval and Guilarte Moreno, 2012). The fitting procedures were carried out with the Microcal OriginPro 9.5 software using a Levenberg-Marquardt algorithm by chi-square minimisation. For the Al centre, an exponential+linear function (EXP+LIN) was fitted through the data points (see equation in Duval et al., 2017a), and data were weighted by the inverse of the squared ESR intensity ($1/I^2$). D_E values were obtained by extrapolating the EXP+LIN function to the residual ESR intensity (Table 1), as in the Total Bleach method described in Forman et al. (2000). This approach is based on the assumption that the signal of the Al centre has been fully reset to its residual level during sediment transport (Voinchet et al., 2003 & 2004). If not, then the dose result derived from the Al centre should be interpreted as a maximum possible estimate of the true burial dose. For the Ti centre, we have used the function labelled as Ti-2 in Duval and Guilarte (2015), in order to describe the non-monotonic dose dependence of the ESR signal at high doses. Data were weighted by the inverse of the squared experimental error ($1/s^2$) and D_E values were obtained by back extrapolation to Y=0 (Table 2). For each sample, final dose response curves (DRCs) were obtained by pooling all the repeated measurements in a single plot (Supplementary material, Fig. S3 and S4), as recommended by Duval (2012). The final 1σ D_E error is derived from the combination of the errors on the fitting and on the calibration of the irradiation source (2.3 %).

The total dose rate value was derived from a combination of *in situ* and laboratory measurements. External gamma dose rates were derived from *in situ* measurements by using the “threshold technique” (Duval and Arnold, 2013). For each dated sample, the corresponding radioelement (U, Th, K) concentrations in the raw sediment were determined by ICP-MS analysis of about 5 g of dry material (Supplementary material, Table S3). Concentration values were used to derive external alpha and beta dose rate components using the dose rate conversion factors from Guérin et al. (2011). Potential disequilibrium in the U-238 decay chain was not directly evaluated. Nevertheless, the consistency between the gamma dose rate values derived from *in situ* and laboratory measurements may be used as a good proxy to suggest the negligible impact of such disequilibrium, if present. Dose rate values were calculated assuming a mean grain size of 150 µm, and an assumed thickness removed by HF etching of 20 µm. Internal dose rate was assumed to be 50 ± 30 uGy/a as in Duval et al., (2017). Values were corrected with beta and alpha attenuation values for spherical grains (Brennan et al., 1991; Brennan, 2003) and water attenuation formulae from Grün (1994). Actual water contents were evaluated in the laboratory by drying the sediment at 50 ºC in an oven during three weeks. Results vary within a relatively narrow range from 7 to 12 % (wet weight) among the samples. These values most likely underestimate the long-term water content at these sites, because the samples were collected at shallow depths from the section surface (<30 cm). Some drying out of the sediment profiles may have occurred prior to sampling because these sections had been exposed for several years in the excavation area. For these reasons, dose rate evaluation was performed with higher assumed values of 20 ± 5%, which is consistent with the 21-22% (% of dry sediment weight) used for the TT-OSL dating comparisons at BN and LTS. The large associated error (5% at a 1σ confidence level) covers a range from 10 to 30% at 2σ, most likely encompassing any significant long-term variability of the water content. The cosmic dose rate was calculated using formulae from Prescott and Hutton (1994), with depth, altitude and latitude corrections (Prescott and Hutton, 1988).

ESR age calculation were performed using ESR-Qz, a non-commercial SCILAB based software, with error calculations based on Monte Carlo simulations, considering the following sources of uncertainties: concentrations, depth, water content, gamma dose rate, beta dose attenuation, D_E values. Test comparisons performed with DRAC (Durcan et al., 2015) show that both programs provide very close results for a given data set (Kreutzer et al., 2018). ESR ages are given with 1σ error ranges (Table 3).

3.2. Extended-range luminescence dating

The comparative extended-range luminescence dating study at BN and LTS focuses on single-grain TT-OSL dating of quartz, following the successful application of this approach at several independently dated Lower Palaeolithic sites from southwest Europe (e.g., Demuro et al., 2014; Arnold et al., 2013, 2014; Arnold and Demuro, 2015). Single-grain TT-OSL dating was performed at the CENIEH Luminescence Dating Laboratory, Burgos, Spain, using the instrumentation, methodological procedures and TT-OSL quality assurance criteria outlined in Arnold et al. (2014).

TT-OSL equivalent dose (D_E) values were determined using the single-aliquot regenerative-dose (SAR) protocol shown in Table S4, which has been modified to enable measurement of individual quartz grains. The suitability of the chosen D_E determination procedures was assessed by undertaking a 2000 Gy dose-recovery test on sample CRF11-4, following the approach outlined in Bartz et al. (2019). A net (i.e., natural-subtracted) measured-to-given dose ratio of 1.00 ± 0.06 was obtained for this sample, confirming the suitability of the SAR procedure under controlled laboratory conditions.

'Pseudo' single-grain TT-OSL D_E measurements have been made by loading 125-180 um quartz grains into standard single-grain aluminium discs drilled with a 10×10 array of 300 µm-deep depressions (holes). It is estimated that ~7 grains are placed in each hole when using this configuration (Arnold et al 2012a), though we are reasonably confident that true single-grain resolution has been maintained in this study owing to the low frequency of grain-hole positions that produce TT-OSL signals (62-67% of measured grain-hole positions did not produce any statistically distinguishable TT-OSL T_n signals for samples CRF11-2 and CRF11-4; Table S5). Individual D_E values were obtained from the first 0.17 s of laser stimulation with a background subtraction derived from the last 0.25 s of stimulation.

Following the findings of Bartz et al. (2019), we have used an additional Fast Ratio (FR) (Durcan and Duller, 2011) quality assurance criteria to ensure that potentially unsuitable grains displaying very slowly bleaching TT-OSL signals are not included in our final age assessments. The FR has been calculated by comparing the counts in the initial channel (0.017 s) of the TT-OSL decay curve (L_1) with those in the middle part of the decay (average counts over 1.0–1.2 s; L_2) after subtracting a late light background count from the last 0.068 s (L3), according to the equation $(L_1-L_3)/(L_2-L_3)$. Sensitivity tests involving assessments of increasingly stringent FR threshold versus weighted mean D_E (e.g., Bartz et al., 2019) revealed that a FR acceptance threshold of ≥20 was suitable to eliminate any potentially biasing effects associated with slow decaying TT-OSL signals for these particular samples (Arnold et al., in prep).

Environmental dose rates have been calculated using a combination of *in situ* field gamma-ray spectrometry (e.g., Arnold et al., 2012b) and low-level beta counting (Bøtter-Jensen and Mejdahl, 1988), taking into account cosmic-ray contributions (Prescott and Hutton, 1994), an assumed minor internal alpha dose rate (Bowler et al., 2003), beta-dose attenuation (Mejdahl, 1979; Brennan, 2003) and long-term water content (Aitken, 1998). Further details of the dose rate determination procedures are provided in Table 4.

3.3. Palaeomagnetism

All magnetic measurements were carried out in the Paleomagnetism Laboratory at the CENIEH. Analyses included measurement of the magnetic remanence in a shielded, three-axis superconducting 755R-4K rock-magnetometer (2G Enterprises). Samples were demagnetized using standard procedures including both thermal and alternating field demagnetization, based on previous results from similar lithologies (Parés et al., 2018). Additional rock-magnetic analyses include isothermal remanent magnetization, and hysteresis cycles, carried out to determine the magnetic mineralogy that is responsible for the paleomagnetic signal. Characteristic Remanent Magnetization (ChRM) component directions were calculated for all specimens using Principal Component Analysis, guided by visual inspection of orthogonal ("Zijderveld type") demagnetization plots (Zijderveld, 1967). Mean directions and associated statistical parameters were estimated using Fisher's method (Fisher, 1953). Corresponding Virtual Geomagnetic Pole Latitude was used to determine the magnetic polarity at each sampling horizon (Supplementary Material Fig. S8).

4. Results

4.1. ESR dating

4.1.1. D_E determination

4.1.1.1. Al centre

ESR data derived from the measurement of the Al centre are displayed in Table 1. Bleaching coefficients values vary between 50% and 60%, suggesting somewhat similar bleaching conditions for all samples. As a comparison, these values are close to those obtained from other samples located within the Iberian Peninsula, such as those from Cuesta de la Bajada or the Alcanadre fluvial terraces (55-60%, Duval et al., 2015; Duval et al., 2017a).

The quality of the ESR data collected is within acceptable standards when compared with previous studies. Measurement repeatability for a given sample is <4 %, except for sample LUN1103 (7.4%). This results in a higher D_E variability of 13% over repeated measurements, while it remains <10% for the other samples. Goodness-of-fit is excellent for 3/4 samples with adjusted r^2 >0.99. The remaining sample (NOI1104) has a slightly lower adjusted r^2 value as a result of some scattered points in the lowest part of the curve (Fig. S3).

In summary, there is a series of consistent evidence (measurement and D_E variability, high goodness-of-fit) indicating the overall quality and reliability of the ESR dataset collected for these four samples.

4.1.1.2.Ti centres

The quality of the ESR data collected for the Ti-Li centre (option D) is good overall. Measurement repeatability achieved for the four samples is <1.5 % (Table 2). The variability of the D_E values is good (<10%) for 2 of the 4 samples, while the remaining two samples display higher values of around 15-16%. Goodness-of-fit is generally relatively good (Fig. S4), with 3 samples displaying adjusted r^2 values between 0.98 and 0.99 and the last one >0.99.

Option A yields higher D_E estimates for 3/4 samples, with the exception being NOI1101 (Table 2). This pattern is consistent with previous observations by Duval and Guilarte (2015), and is due to the influence of the peak at g=1.979 (option E). The latter provides systematically higher D_E estimates (between +33% and 48% higher than option D). Previous studies have shown the potential of Option D for providing accurate age estimates in agreement with independent age control (e.g. Duval et al., 2017a; Bartz et al., 2018; Mendez-Quintas et al., 2018). Consequently, the final ESR ages were derived from Option D in the present study. The ESR fitting results derived from the other options are nevertheless made available in Table 2 so that the corresponding ages can be calculated and referred to in future studies if required.

Finally, it should be mentioned that D_E estimates were also obtained from Option C (Ti-H) for comparison, but discarded for age calculation. Goodness-of-fit was found to be lower than for Options A and D (0.96 < adj. r2 < 0.99), and the resulting D_E estimates were found to be between 40% and 75% lower than those obtained with Option D. Although the Ti-H centre has been recently found to show great potential to date late Middle to Late Pleistocene deposits (e.g. Kreutzer et al., 2018; Mendez-Quintas et al., in prep.), it is still unclear whether it can be reliable for older samples, and in particular for D_E values > 1000 Gy (Duval and Guilarte, 2015), as is the case in the present study.

4.1.1.3.The MC approach

The Al centre provides systematically higher D_E estimates (between +4 and 32 %) compared with Ti-Li centre Option D, although one may reasonably consider that NOI1101 yields Al results within error of its corresponding Ti-Li results (Tables 1 and 2). Following the principles of the MC approach, this pattern indicates that the ESR intensity of the Al centre was not fully reset during sediment transportation (with the exception of sample NOI1101), as the result of its slower bleaching rate when compared with that of the Ti centres (see Fig. 1 of Duval et al., 2017a).

4.1.2. ESR age estimates

The two samples from LTS provide ESR ages within error for a given centre: ~850-900 ka for the Al centre and ~650-730 ka for the Ti-Li centre (Table 3). These results suggest that Units 1 and 3 may be considered as almost coeval. In comparison, the ESR-Al ages obtained at BN provide a maximum possible chronology for the deposits ranging from ~680 to ~940 ka from top to bottom. In contrast, the Ti centre yields somewhat younger ages of ~650 to ~740 ka that are within error of each other, suggesting a rapid sedimentation for the different layers.

In accordance with the MC approach, the results derived from the Al centre are interpreted as maximum age constraints for the samples, while the Ti-Li centre is considered to provide a more accurate estimate of the burial age of the deposits.

4.2. Single-grain TT-OSL dating

The single-grain TT-OSL dating results are summarised in Table 4. Single-grain TT-OSL measurements were made on 1900-2000 quartz grains per sample, with ~10% of these individually measured grains deemed suitable for D_E determination after applying the single-grain quality assurance criteria of Arnold et al. (2014) and a FR acceptance threshold of ≥20 (Table S5). Representative decay and dose-response curves for two accepted grains are shown in Supplementary Material Fig. S5. The single-grain TT-OSL dose-response curves for samples CRF11-2 and CRF11-4 are all well-represented by a single saturating exponential function, and exhibit continued signal growth over high dose ranges of several kGy.

The single-grain TT-OSL D_E distributions of CRF11-2 from LTS Unit 3 and CRF11-4 from BN layer *a* display limited scatter and contain a single dose population, with the vast majority of individual D_E values being well represented by the weighted D_E value (falling within the shaded band in the radial plots) (Supplementary Material Fig. S6). Neither of these samples are considered to be significantly positively skewed according to the criterion outlined by Arnold and Roberts (2011). Low to moderate overdispersion values of 29 ± 4% and 34 ± 5% were obtained for samples CRF11-2 and CRF11-4, respectively, which are in agreement at 2σ with values reported elsewhere for well-bleached and unmixed single-grain TT-OSL samples (e.g., 21 ± 2%; Arnold et al., 2019). These D_E distribution characteristics suggest that the LTS and BN TT-OSL samples were not significantly affected by partial bleaching or any major post-depositional complications thereafter (e.g., sediment mixing or beta dose rate heterogeneity).

Consequently, representative single-grain TT-OSL burial dose estimates have been calculated using the central age model (CAM) of Galbraith et al. (1999).

4.3.Palaeomagnetism

Initial Natural Remanent Magnetization (NRM) intensities were on the order of 10^{-3} to 10^{-4} A/m, which is well-above the noise level of the cryogenic magnetometer. Both thermal and AF demagnetization were used to isolate the Characteristic Remanent Magnetization (ChRM), although the former was proven to be more efficient at isolating the ChRM directions. Demagnetization plots (Supplementary Material, fig. S7) reveal a secondary, soft magnetization component in many samples. Such viscous magnetization is typically erased by heating to 200-300^{o}C . After removal of this secondary component, a ChRM direction was defined. Most samples produced stable, well-defined ChRM directions, with maximum angular deviation below 15^{o} (see Table 5). Only normal polarity directions (north seeking and downwards) were obtained using either method (thermal or alternating field), giving confidence of the effectiveness of the cleaning procedure (Supplementary Material, fig. S8). Specimens from sampling site LUN1 are an exception. Only two specimens produced interpretable demagnetization paths, albeit they are somewhat noisy. Unfortunately, the lack of enough vectors hampers computing a reliable linear regression for these specimens from LUN1. It is noteworthy that after a strong overprint (up to 300-400 ^{o}C), some vectors above 450 ^{o}C suggest the presence of a higher stability component in the south quadrant, perhaps revealing a south-directed component strongly masked by the normal magnetic field. We have not calculated ChRM directions for these two samples, which will not be further considered. Samples from NOR1-6 sampling site did not produced any stable directions and therefore are not included in the discussion.

Maximum unblocking temperatures and coercivity spectra suggest that (low-Ti) magnetite is the main mineral responsible for the stable magnetization, with some contribution of hematite.

5. Discussion

5.1. ESR age comparisons

5.1.1. Al centre

In general, the ESR-Al results obtained for CENIEH and MNHN samples at LTS are in agreement at 2σ and indicate an Early Pleistocene chronology for the deposits of Units 1 and 3

(Fig. 5). However, closer evaluation of the two ESR-Al datasets reveals a noticeable age difference. The CENIEH ESR sample LUN1103 from Unit 1 provides an age estimate of 893 ± 87 ka, which is in good agreement with the two MNHN ESR results available (black circles in Fig. 5B: 808 ± 71 and 839 ± 79 ka; Table S1). In contrast, the ESR-Al age of LUN1101 (866 ± 100 ka) from the bottom of the local sequence is > 200 ka younger than the three closely associated MNHN ages from Unit 3 (black circles in Fig. 5A: 1102 ± 119, 1174 ± 122 and 1227 ± 123 ka; Table S1). This age difference is most likely linked to the D_E evaluation, and especially to the fitting function used. This hypothesis is confirmed by the new D_E evaluations performed using the EXP+LIN fitting function for the MNHN samples (red circles in Fig. 5A and B; numerical values are given in Table S1) as recommended by Duval (2012): while samples from Units 1 and 2 are largely insensitive to the use of this fitting function (±1% and -4%, respectively; Table S1) those from Unit 3 yield significantly younger ages (by 100-230 ka, or -8 to -26 %; Table S1). The resulting ages of the Unit 3 samples range from 900 to 1100 ka when using the EXP+LIN fitting function (red circles in Fig. 5A). These results are, within error, in good agreement with the CENIEH ESR-Al age estimate of 866 ± 100 ka obtained for sample LUN1101, which is also based on the use of an EXP+LIN fitting function. The reduction of the D_E value induced by the use of the EXP+LIN function is consistent with the results obtained by Duval (2012) from a previous comparison study based on 15 quartz samples. In that study, the D_E values derived from the EXP+LIN function were on average 33% lower than those obtained from the SSE function. The magnitude of this systematic difference was nevertheless sample-dependent (ranging from -64 to -8% depending on the sample considered), which may explain why some MNHN samples are significantly less affected by the choice of the fitting function.

Figure 5 approx. here

At the BN locality, CENIEH sample NOI1101 from the top of layer *b* provides an Al age of 682 ± 68 ka, which is not only consistent with the nearby Cher2004-11 and Cher2004-12 sample ages (699 ± 76 and 680 ± 77 ka; Table S2 & Fig. 4) but also with all the MNHN ESR age estimates obtained for that layer (red circles in Fig. 5D). In contrast, the age of 940 ± 110 ka obtained for CENIEH sample NOI1104 at the base of the sequence is significantly older than that obtained for the stratigraphically associated MNHN ESR samples from the upper part of layer *a* (*a2*) (red circle in Fig. 5C: 645 ± 30 ka). This apparent age discrepancy most likely originates from the D_E values: these differ significantly by ~40% (1875±87 Gy vs. 2639±263 Gy), while both samples display similar dose rate values (2907±40 µGy/a vs. 2807±221 µGy/a). Interestingly, the bleaching coefficient of 57% measured for NOI1104 (Table 1) is much higher than that obtained for the MNHN sample (42%; Table S1). This suggest different bleaching conditions for the two samples and different levels of ESR signal resetting was achieved for the Al centre during sediment transport. Consequently, we consider that the apparent age discrepancy is most likely due to lateral variations of the slope deposits at BN (see Fig. 6 and 8 from Despriée et al., 2017b), whose complexity cannot be easily captured in such generalised or composite stratigraphic logs. The MNHN and CENIEH samples were not collected at the exact same spot within each layer, but were laterally distant by a few meters. Consequently, the dose scatter (and the resulting age discrepancy) may simply be the result of the heterogeneity of the sandy matrix within slope deposits that may not have locally experienced enough transport and/or sunlight exposure to fully reset the ESR-Al signal of sample NOI1104.

In summary, the CENIEH and MNHN samples provide ESR-Al ages that are within error of each other for 3/4 of the samples considered in this study. These results show that ESR dating performed by the two independent laboratories yield generally reproducible chronologies.

5.1.2. Ti-Li centre

The Ti-Li ESR ages derived from the CENIEH samples provide an additional age constraint for the deposits. In accordance with the basic principles of the MC approach, the Al centre is considered to provide a maximum possible chronology for the deposits given the differences observed in the D_E estimates derived from each centre, while the Ti-Li chronology most likely represents the closest estimate for the true age of sediment deposition. This, however, does not mean that Al results measured in isolation (i.e., not as part of the MC approach) should automatically be interpreted as systematically overestimating the true age of the deposits. Recent studies have indeed demonstrated that this approach may sometimes provide ages in agreement with independent age control (e.g. Pereira et al, 2018; Duval et al 2015). Nevertheless, 3 out of 4 samples in the present study show overestimated Al ages, i.e. $\geq$100 ka older than their Ti-Li equivalent (Fig. 5), while, interestingly, one sample from the upper part of the sequence at BN site shows consistent Al and Ti-Li ESR ages (NOI1101, Fig. 5D). In this case, the combined Al-Ti-Li CENIEH age (Al: 682 ± 69 ka; Ti: 653 ± 63 ka) is also in agreement with the ESR-Al MNHN samples from the same layer (680 ± 77 and 699 ± 76 ka). In contrast, sample NOI1104 at the bottom of the sequence yields an ESR-Al age of 940 ± 118 ka, which is about 200 ka older than the corresponding Ti-Li estimate (Fig. 4 & 5C). Here, in accordance with the principles of the MC approach, the difference given by the two centres may be interpreted as evidence of the very limited transport experienced by the slope deposits, i.e. insufficient resetting of the Al signal due of its significantly slower bleaching kinetics (e.g. Duval et al., 2017a). The CENIEH Ti-Li age of 739 ± 72 is also consistent at 1σ with the MNHN ESR age of 645 ± 30 ka from the same layer *a2* (Fig. 5C) and with the other 6 ESR ages from *b* above. These new results support the previous chronological assignment of ~700 ka for the Acheulean artefacts made by Moncel et al (2013).

At LTS, the Ti-Li ages provide an overall younger chronology (~650-730 ka) compared with the previous MNHN ESR-Al ages and the newly obtained CENIEH ESR-Al ages, which both indicated an Early Pleistocene chronology of around 800-1200 ka and 800-900 ka, respectively, for the sequence (Figs. 3, 5A & 5B). In accordance with the basic principles of the MC approach, the Ti-Li chronology is in the first instance considered to represent the closest estimate for the true age of sediment deposition. The accuracy of these results can, however, only be evaluated by cross-comparison with independent age control.

5.2. Independent age control

The new single grain TT-OSL and palaeomagnetic data collected in the present study, together with the TCN results published previously by Shen et al (2012), provide stratigraphically well-constrained independent age control against which the ESR chronology can be compared. Most notably, the ESR-Ti ages are consistent at 1σ with the paired single-grain TT-OSL ages derived from closely associated samples at both sites: 739 ± 72 ka (ESR-Ti) vs. 644 ± 47 ka (TT-OSL) for BN layer *a*, and 654 ± 64 ka (ESR-Ti) vs. 727 ± 51 ka (TT-OSL) for LTS Unit 3. Despite their large associated uncertainties, the TCN ages of ~700-750 ka published by Shen et al (2012) are also consistent with the TT-OSL and ESR-Ti data.

In summary, the numerical ages obtained using three independent radiometric dating techniques collectively point to an early Middle Pleistocene chronology for the dated deposits at BN and LTS. These numerical chronologies are also supported by the palaeomagnetic data, which yielded a normal polarity for all of the samples collected at the two sites, and thus suggests that the deposits formed during the Brunhes chron (<772 ka; Okada et al., 2017).

5.3. Evaluating the impact of potential laboratory biases on the ESR age results

The absence of proper standardization regarding laboratory practices and dose rate evaluation in the field of ESR dating results in significant variability in the methodologies employed by different dating laboratories and research groups. Inter-laboratory comparisons performed on known-age samples and under well-controlled experimental conditions are essential for examining any potential laboratory bias induced by the use of different methodologies. Unfortunately, such inter-laboratory comparisons are virtually non-existent with regards to ESR dating of optically bleached quartz grains. The present work is perhaps one of the closest attempts to undertake an inter-laboratory comparison study (see also Bahain et al., accepted), although it should not strictly be considered as such, given the time elapsed between sampling by the two labs, and the random lateral distances between sampling positions at each locality. Closer examination of the data produced by each laboratory shows that the CENIEH samples display both lower D_E and dose rate values compared to their MNHN equivalents. However, any further data comparison is made complicated by the fact that these samples have been collected and processed in a totally independent way. In other words, it should be kept in mind that the differences observed may be either due to local/lateral variability within the sampled layer, or to the specific analytical procedure employed by each laboratory.

In particular, although the CENIEH ESR samples and their MNHN equivalents can be stratigraphically positioned within the same layers, they were not collected next to each other and there is thus an inherent uncertainty on the comparative dose rate and D_E values. Additionally, we have identified several differences in the analytical procedures employed and assumptions considered by the two laboratories. These differences are related to, among other things, the internal dose rate (MNHN: null; CENIEH: 50 ± 30 µGy/a), the water content considered for the dose rate evaluation (MNHN: measured values between 10% and 15% (LTS) or assumed to 10% (BN); CENIEH: assumed to 20 ± 5%), the *in situ* measurement of the gamma dose rate (MNHN: systematic but posterior to the sampling; CENIEH: systematic and at the same time as the sampling), and the choice of the fitting function used for the D_E evaluation of the Al centre (MNHN: Single Saturating Exponential (SSE) for the LTS samples and EXP+LIN for the BN samples; CENIEH: EXP+LIN for all samples). Some of these differences are naturally explained by the recent methodological developments that have taken place since the publication of the MNHN ages (e.g. the systematic use of the EXP+LIN function for the Al centre), while others are due to distinct conventions or practices applied by each laboratory in the dose rate evaluation. It is beyond the scope of the present study to discuss the validity of each approach. However, sensitivity tests can nevertheless be performed to evaluate their impact on the calculated ESR age results (Fig. 6). For example, the assumptions around the internal dose rate carry very little weight in the total dose rate evaluation: when assumed to be null (like for the MNHN samples), the CENIEH ESR age results become slightly older (by only 2%; Fig. 6). In comparison, when considering a water content of 10% for the four CENIEH samples (i.e., similar to that used for most of the MNHN samples; Tables S1 & S2), the ESR age estimates become younger by 12% on average; though they remain within error of the original calculations (Fig. 6). These revised ages would still be in agreement with the MNHN age results for 3/4 samples, and the overall age difference would even be reduced for LUN1103, NOI1104 & NOI1101 (Fig. 5).

Figure 6 approx. here

In summary, we have identified a series of differences between the methodologies employed by each laboratory. Although these differences have an apparent impact on the calculated ESR age estimates, they do not induce any statistically significant bias between the CENIEH and MNHN samples, which yield generally reproducible results.

5.4. Implications of the new dating results

The results of the present dating study provide significant advances for understanding the chronology of the two sites and the fluvial formations associated with the Cher River in general. At LTS, these results challenge current understanding of the site formation and stratigraphy, whereas at BN they strongly support previously published chronostratigraphic data.

5.4.1. Chronology of the fluvial formations associated with the Cher river

5.4.1.1. Unit 1 at LTS

The MNHN ESR-Al ages are consistent at 1σ with both the new CENIEH ESR-Ti ages and the palaeomagnetic results, indicating a Brunhes age (< 772 ka) for the fluvial deposits of layer b. In contrast, the ESR-Al age of 893 ± 87 obtained for LUN1103 appears overestimated, most likely as the result of incomplete resetting of the Al signal during transport. Consequently, a mean age of 792 ± 57 ka (n=3, 1 s.d.; Fig. 7) may be obtained for Unit 1 at LTS (Fig.7). This result is consistent with the chronology of 816 ± 71 ka (Despriée et al., 2011; see also Fig. 1), previously established for fluvial terrace E (+29-34 m) (Despriée et al., 2011; see also Fig. 1). However, the additional age constraint given by the palaeomagnetic data enables unequivocal correlation of the fluvial deposits to the earliest part of the Middle Pleistocene, i.e. specifically to a time interval of between 735 and 772 ka (considering the lower 1σ uncertainty range of the mean ESR age; Fig.7). Consequently, these results indicate that fluvial deposits at LTS (Unit 1) may result from an aggradation phase around the interglacial/glacial transition associated with MIS19-18. This is consistent with the model of river response typically proposed for terrace system formation in north-west Europe (e.g. Antoine, 1994; Bridgland, 2000), which is mostly driven by cyclic climatic fluctuation.

Figure 7 approx. here

5.4.1.2.Unit 3 at LTS

The present dating study sheds new light on the chronology of the fluvial deposits (layer b) of Unit 3 at LTS. Independent results derived from single-grain TT-OSL, TCN and ESR-Ti methods are all consistent and provide a mean age of 710 ± 50 ka (n=3; 1 s.d.). This combined age estimate is within error of the chronology obtained for Unit 1 (735-772 ka) and consistent with a correlation to MIS19-18 or MIS17-16 interglacial-glacial cyclicity. As detailed above (section 5.1), two main reasons may explain the significantly older ages previously obtained for Unit 3 using the ESR-Al centre (~1.1-1.2 Ma; Despriée et al., 2011): the use of a different function to fit the experimental data points derived from the measurement of the Al centre, and incomplete resetting of the ESR signal associated with the Al centre during sediment transport.

These new dating results raise many questions around the local chronostratigraphic interpretation of the deposits. They indicate that the time interval between Unit 1 and 3 is significantly shorter (20-60 ka) than initially assumed (>300 ka; Despriée et al., 2011). Units 1 to 3 have been initially correlated to three fluvial terraces E, F and G (e.g. Despriée et al., 2011). However, given the uncertainty ranges of the new dating results (735-772 ka for Unit 1 and 710 ± 50 ka for Unit 3), it can now be reasonably envisaged that the three units are almost coeval. Sedimentological evidence indicates that the three units are most likely not part of the same depositional event, because they display very different sandy sedimentary facies (Unit 3: indurated coarse red sands with a high proportion of clays; Unit 2: horizontally laminated beige sands typical of torrential flow; Unit 1: fine and laminated fluvial sands). The combination of these field observations with the newly obtained dating results suggest that the fluvial deposits in each unit most likely correspond to different short aggradation events within the main aggradation phase associated with the formation of fluvial terrace E (e.g., Bridgland and Westaway 2008).

Another hypothesis would be to consider that deposits from Unit 3 are indeed much older than those from Unit 1, but have been reworked and exposed to sunlight about 710 ka ago. However, the available chronological data do not support this possibility. The TT-OSL sample CRF11-2 does not show high D_E overdispersion values that could indicate partial bleaching or different populations of grains with different bleaching history. Additionally, the independent age control provided by the TCN method also points towards a Middle Pleistocene chronology.

On the one hand, these unexpected young numerical dating results may contradict the initial correlation of the sandy Units 1, 2 and 3 to the Sables-de-Rosières Formation, which delivered the only fossil assemblage in the area at Lunery Rosières-Usine site (Despriée et al., 2017). Its age, inferred from biochronology, is estimated to be around 1 Ma based on the similarities with other sites such as Le Vallonnet or Saint Prest (Guérin et al., 2003). Such an inference should nevertheless be considered with caution, not only because of the inherent uncertainty associated with biochronology, but also due to the existing uncertainty in the taxonomic attribution of some species, as mentioned by Guérin et al. (2003). However, on the other hand, stratigraphic and sedimentological evidence at LTS suggests the presence of a major unconformity between layers *a* and *b* (see Despriée et al., 2017a), which may indicate a significant chronological gap. It is possible that the fluvial sediment originally deposited on top of *a* has been fully eroded and replaced by much younger fluvial deposits from a subsequent aggradation phase. This would explain the apparent discrepancy between the biochronology and the numerical age results obtained in the present study. However, it is difficult to test this hypothesis further, given the absence of suitable material in layer *a* for numerical dating, and also because both Rosières-Usine and the LTS sites are no longer accessible.

5.4.1.3 Layer b at BN

At BN, all of the ESR results (CENIEH and MNHN, Al and Ti) obtained for the fluvial deposits of layer b are consistent at 1σ. They provide a mean age of 665 ± 29 ka (n=8; 1 s.d.) for fluvial terrace D (+14-21 m) of the Cher Valley (Fig.7), which is virtually the same as published earlier (665 ± 55 ka, Despriée et al., 2011; see also Fig. 1). These combined dating results indicate that the fluvial deposits of layer b accumulated around MIS 17-16, which is consistent with the main aggradation phase defined by Bridgland (2000) at the interglacial-glacial transition. Alternatively, following the terrace formation system described by Antoine, (1994) for the nearby Somme valley, these fluvial deposits may be correlated to glacial conditions prevailing during MIS16 (Despriée et al., 2017c).

5.4.2. The age of the lithic assemblages at BN and LTS

Because the lithic tools found at BN and LTS have not been directly dated by numerical means, the age of the hominin occupations must be inferred by integrating the existing numerical dating, sedimentological and stratigraphic evidence. To do so, a couple of key questions should be answered for each site: (i) to what extent are the artefacts found in *in-situ* position and have any been reworked from other deposits? (ii) to what extent can the numerical ages constrain the true age of the hominin occupation/presence ?

The study of the lithic assemblages at LTS and BN localities suggest that the artefacts underwent minimum transport and that both assemblages were found in primary position. Prehistoric artefacts were knapped on siliceous blanks (millstone slabs and weathered Jurassic silicifications) gathered on the incision floor by hominins from the coarse slope deposits coming from the plateau. The presence of cores, chopper-cores and flakes suggest that both were workshop sites (e.g. Despriée et al., 2011). Additionally, the study of naturally accumulated cobbles at BN has led to the identification of a series of features that are typical of repeated high-energy fluviatile-type transport (Despriée et al., 2016). In contrast, the lithic artefacts show knapped ridges that are not blunted and cutting edges that are not crushed, suggesting that they experienced very little, if any, transport. Similarly, at LTS, the artefacts show no evidence of surface abrasion as the result of a transport (Despriée et al., 2011). Consequently, there is no evidence to suggest that archaeological levels should be interpreted as palimpsests. The data collected from fieldwork observations and laboratory analyses suggest that the artefacts were protected from the subsequent glacial frost effects by the cover of new solifluction deposits, which were in-turn followed by the fluvial sandy deposits that currently overlie the archaeological levels (Despriée et al., 2017a and b). The main question lies now in evaluating the time elapsed between the production of the lithic assemblages and the subsequent accumulation of the slope and fluvial deposits.

At BN, the fluvial deposits associated with layer *b* provided a mean age of 665 ± 29 ka, which should thus be interpreted as a minimum age constraint for the Mode 2 lithic assemblage found stratigraphically below, within layer *a*. Numerical dating of the slope deposits of layer *a2* post-dating the archaeological artefacts yields a mean age of 690 ± 52 ka (n= 4: TT-OSL, CENIEH_ESR-Ti, MNHN_ESR-Al and TCN; 1 s.d.). This result is stratigraphically consistent with that of layer *b*. It provides an additional minimum age constraint for the lithic assemblage. General interpretation of the site formation suggests that this accumulation was deposited after the end of river incision, i.e. at the beginning of a glacial period based on the model proposed by Antoine (1994) for the nearby Somme valley, and locally underwent cryoturbation together with the altered limestone level during the glacial maximum (Despriée et al., 2007b). Consequently, given the existing age uncertainty, the beginning of MIS16 around 676 ka (Lisiecki and Raymo, 2005) may provide a maximum age constraint for the diamicton at the bottom of the sequence, while the 1-σ upper range of the mean age (690-52 = 638 ka) may be used as a minimum age constraint. Therefore, an age range of 676-638 ka may be proposed for the hominin occupation at BN (Fig. 7). This result is consistent with the initial chronology proposed by Moncel et al (2013) and confirms that BN is among the oldest Acheulean occurrences in Western Europe north of the 45°N latitude (see also Antoine et al., 2019).

At LTS, the mean age of 710 ± 50 ka obtained for the sandy layer *b* provides a minimum age constraint for the archaeological level located below. Despriée et al., (2017a) position the hominin presence at the end of the incision phase, which might have occurred during the earliest part of MIS 18 following the model by Antoine (1994). However, the detailed stratigraphic profile of the excavation suggests a major disconformity between the pebble layers hosting the lithic artefacts within *a* (labelled c0, c1 and c2 in Despriée et al., 2017a) and the fluvial deposits associated with layer *b*. Consequently, it may reasonably be envisaged that deposits from layers a and b were not deposited during the same aggradation phase. If so, then the chronological gap between these layers might be significant, which would imply that the estimated age of the lithic assemblage at LTS is much older than 710 ± 50 ka. Indeed, the major technological and typological differences between the lithic assemblages at LTS and BN might also be considered as indirect evidence to support this hypothesis. At LTS, the lithic assemblage is made of choppers, chopper-cores on cobbles with small flakes (Mode 1) and without bifacial pieces or large cutting tools. In contrast, the assemblage from BN contains only cores on millstone slabs with flakes, and numerous Acheulean handaxes and large cutting tools (Mode 2). These significant differences between both assemblages is more likely to be explained by a major chronological gap between the two occupations than by the opportunistic behaviour of hominins in the earliest part of the Middle Pleistocene. Technological and typological characteristics of the lithic artefacts found at LTS fall within the variability of the Mode 1 assemblages described at the Early Pleistocene sites of Europe (see section 6.3 in Despriée et al., 2017a). Consequently, a comparable minimum age of 0.8 Ma may reasonably be inferred for the lithic assemblage of Unit 3 at LTS, which is consistent with the minimum age of 710 ± 50 ka suggested in the present work. Cryoturbation features affecting the accumulation of blocks, cobbles and pebbles at the bottom of Unit 3 document the occurrence of a cold climate that could be tentatively linked to a glacial stage of the late Early Pleistocene (e.g., MIS20, MIS22?). However, in the absence of direct age control for the deposits of layer a, there is, for the moment, no clear evidence supporting a correlation of hominin presence at LTS to a given

MIS. Any further attempts at refining the chronological constraint of Unit 3 would become too speculative.

Conclusion

The dating results of the present study have not only helped to further constrain the chronology of the fluvial deposits from the Cher river, one of the Loire tributaries, but they have also shed new light on the age of two key Lower Palaeolithic sites located in central France: Lunery-La Terre-des-Sablons and Brinay-la Noira. Hominin presence at BN may tentatively be correlated to the early MIS16 (676-638 ka), which is in agreement with previous interpretations. In contrast, only a minimum age of ~710 ka may be securely proposed for hominin presence at LTS, although an Early Pleistocene chronology may not be discounted based on stratigraphical and technological evidence. Unfortunately, any future attempt to obtain additional chronological constraints is almost impossible as the site is no longer accessible.

The present study is another example showing the importance of using the Multiple Centre approach in ESR dating of quartz (e.g. Duval et al., 2017a; Kreutzer et al., 2018; Mendez-Quintas et al., 2018), which remains the best way to evaluate potential incomplete resetting of the ESR-Al signal. Finally, given the inherent non-negligible uncertainties associated with the use of dating methods such as ESR, luminescence and TCN, the multi-technique dating approach used here is undoubtedly the most appropriate way to build more robust and accurate chronologies for Early to Middle Pleistocene archaeological sites found in fluvial sedimentary environments. The conditions needed for applying this type of multi-technique dating approach are frequently met at Lower Palaeolithic sites located in the Mediterranean region, providing an invaluable means of maximising dating reliability in contexts where highly standardized and accurate methods (e.g., radiocarbon, U-series or argon-argon dating) cannot be routinely employed.

From a methodological point of view, the dating results presented here are especially encouraging for the reliability of the ESR method applied to optically bleached quartz grains. This is to our knowledge one of the first studies demonstrating that ESR quartz samples independently collected, processed and dated by two different laboratories may produce reproducible ESR age results. This kind of comparative work is essential to strongly position the ESR method as a reliable alternative numerical dating method in Quaternary studies.

Acknowledgement

The study was funded by project CGL2010-16821 from the Spanish Ministry of Science and Innovation and Australian Research Council (ARC) Future Fellowship Grant FT150100215. Walter Minnella’s research stays at CENIEH were covered by the Lifelong Learning Programme Erasmus Placement program granted to University of Catania, and the EARTHTIME-EU - Exchange Grant #4569 from the European Science Foundation. Additional financial support for the TT-OSL dating research was provided by Australian Research Council (ARC) Future Fellowship project FT130100195 and ARC Discovery Early Career Researcher Award DE160100743. Carlos Pérez Garrido is thanked for his assistance with preparing and measuring the luminescence dating samples at the CENIEH luminescence dating laboratory, Burgos, Spain. Finally, the authors would like to thank the three anonymous reviewers for their constructive comments, which have contributed to significantly improve the quality of the manuscript.

References

Aitken, M.J., 1998. An Introduction to Optical Dating: The Dating of Quaternary Sediments by the Use of Photon-Stimulated Luminescence. Oxford University Press, Oxford, 267 pp.

Antoine, P. (1994). The Somme valley terrace system (northern France); a model of river response to Quaternary climatic variations since 800,000 bp. Terra Nova 6(5): 453-464.

Antoine, P.M., Marie-Hélène ; Voinchet, Marie-Hélène ; Locht, Jean-Luc; Amselem, Daniel; Hérisson, David; Hurel, Arnaud; Bahain, Jean-Jacques (2019). The earliest evidence of Acheulian occupation in Northwest Europe and the rediscovery of the Moulin Quignon site, Somme valley, France. Scientific Reports 9: 13091.

Arnold, L.J., Demuro, M., 2015. Insights into TT-OSL signal stability from single-grain analyses of known-age deposits at Atapuerca, Spain. Quaternary Geochronology 30, 472–478.

Arnold, L.J., Roberts, R.G., 2009. Stochastic modelling of multi-grain equivalent dose (De) distributions: implications for OSL dating of sediment mixtures. Quaternary Geochronology 4, 204–230.

Arnold, L.J., Roberts, R.G., 2011. Paper I - optically stimulated luminescence (OSL) dating of perennially frozen deposits in north-central Siberia: OSL characteristics of quartz grains and methodological considerations regarding their suitability for dating. Boreas 40, 389–416.

Arnold, L.J., Demuro, M., Navazo Ruiz, M., 2012a. Empirical insights into multi-grain averaging effects from ‘pseudo’ single-grain OSL measurements. Radiat. Meas. 47, 652-658.

Arnold, L.J., Duval, M., Falguères, C., Bahain, J.-J., Demuro, M., 2012b. Portable gamma spectrometry with cerium-doped lanthanum bromide scintillators: suitability assessments for luminescence and electron spin resonance dating applications. Radiation Measurements 47, 6–18.

Arnold, L.J., Demuro, M., Navazo Ruiz, M., Benito-Calvo, A., Pérez-González, A., 2013. OSL dating of the Middle Palaeolithic Hotel California site, Sierra de Atapuerca, northcentral Spain. Boreas 42, 285–305.

Arnold, L.J., Demuro, M., Parés, J.M., Arsuaga, J.L., Aranburu, A., Bermúdez de Castro, J.M., Carbonell, E., 2014. Luminescence dating and palaeomagnetic age constraint on hominins from Sima de los Huesos, Atapuerca, Spain. Journal of Human Evolution 67, 85–107.

Arnold, L.J., Demuro, M., Parés, J.M., Pérez-González, A., Arsuaga, J.L., Bermúdez de Castro, J.M., Carbonell, E., 2015. Evaluating the suitability of extended-range luminescence dating techniques over Early and Middle Pleistocene timescales: published datasets and case studies from Atapuerca, Spain. Quaternary International 389, 167–190.

Arnold, L.J., Demuro, M., Spooner, N.A., Prideaux, G.J., McDowell, M.C., Camens, A.B., Reed, E.H., Parés, J.M., Arsuaga, J.L., Bermúdez de Castro, J.M., Carbonell, E., 2019. Single-grain TT-OSL bleaching characteristics: Insights from modern analogues and OSL dating comparisons. Quaternary Geochronology 49, 45-51.

Arzarello, M., Marcolini, F., Pavia, G., Pavia, M., Petronio, C., Petrucci, M., Rook, L. and Sardella, R. (2007). "Evidence of earliest human occurrence in Europe: the site of Pirro Nord (Southern Italy)." Naturwissenschaften 94(2): 107-112.

Bahain J.-J., Duval M., Voinchet P., Tissoux H., Falgueres C., Grün R., Moreno D., Shao Q., Tombret O., Jamet G., Faivre J.-P. & Cliquet D. (accepted). ESR and ESR/U-series chronology of the Middle Pleistocene site of Tourville-la-Rivière (Normandy, France) - a multi-laboratory approach. Quaternary International.

https://doi.org/10.1016/j.quaint.2019.06.015.

Bartz, M., Rixhon, G., Duval, M., King, G. E., Álvarez Posada, C., Parés, J. M. and Brückner, H. (2018). Successful combination of electron spin resonance, luminescence and palaeomagnetic dating methods allows reconstruction of the Pleistocene evolution of the lower Moulouya river (NE Morocco). Quaternary Science Reviews 185: 153-171.

Bartz, M., L. J. Arnold, M. Demuro, M. Duval, G. E. King, G. Rixhon, C. Álvarez Posada, J. M. Parés and H. Brückner (2019). Single-grain TT-OSL dating results confirm an Early Pleistocene age for the lower Moulouya River deposits (NE Morocco). Quaternary Geochronology 49: 138-145.

Bermúdez de Castro, J. M., Martinón-Torres, M., Martínez de Pinillos, M., García-Campos, C., Modesto-Mata, M., Martín-Francés, L. and Arsuaga, J. L. (2018). Metric and morphological comparison between the Arago (France) and Atapuerca-Sima de los Huesos (Spain) dental samples, and the origin of Neanderthals. Quaternary Science Reviews.

Bøtter-Jensen, L., Mejdahl, M., 1988. Assessment of beta dose-rate using a GM multicounter system. Nuclear Tracks and Radiation Measurements 14, 187-191.

Bowler, J.M., Johnston, H., Olley, J.M., Prescott, J.R., Roberts, R.G., Shawcross, W., Spooner, N.A., 2003. New ages for human occupation and climate change at Lake Mungo, Australia. Nature 421, 837–840.

Brennan, B.J., 2003. Beta doses to spherical grains. Radiat. Meas. 37, 299–303.

Brennan, B. J., Lyons, R. G., Phillips, S. W. (1991). Attenuation of alpha particle track dose for spherical grains. Nuclear Tracks and Radiation Measurements 18: 249-253.

Brennan, B. J. (2003). Beta doses to spherical grains. Radiation Measurements 37: 299-303.

Bridgland, D.R. (2000). River terrace systems in north-west Europe: an archive of environmental change, uplift and early human occupation. Quaternary Science Reviews 19(13): 1293-1303.

Bridgland, D. and R. Westaway (2008). Climatically controlled river terrace staircases: A worldwide Quaternary phenomenon. Geomorphology 98(3–4): 285-315.

Carbonell, E., Bermudez de Castro, J. M., Pares, J. M., Perez-Gonzalez, A., Cuenca-Bescos, G., Olle, A., Mosquera M., Huguet, R., van der Made, J., Rosas, A., Sala, R., Vallverdu, J., Garcia, N., Granger, D. E., Martinon-Torres, M., Rodriguez, X. P., Stock, G. M., Verges, J.

M., Allue, E., Burjachs, F., Caceres, I., Canals, A., Benito, A., Diez, C., Lozano, M., Mateos,A., Navazo, M., Rodriguez, J., Rosell, J. and Arsuaga J. L. (2008). The first hominin of Europe. Nature 452(7186): 465-469.

Carbonell, E., Barsky, D., Sala, R. and Celiberti, V. (2016). Structural continuity and technological change in Lower Pleistocene toolkits. Quaternary International 393: 6-18.

Demuro, M., Arnold, L.J., Parés, J.M., Pérez-González, A., Ortega, A.I., Arsuaga, J.L., Bermúdez de Castro, J.M., Carbonell, E., 2014. New luminescence ages for the Galería Complex archaeological site: Resolving chronological uncertainties on the Acheulean record of the Sierra de Atapuerca, northern Spain. PLOS ONE 9, e110169.

Demuro, M., Arnold, L.J., Par_es, J.M., Sala, R., 2015. Extended-range luminescence chronologies suggest potentially complex bone accumulation histories at the Early-to-Middle Pleistocene palaeontological site of Huéscar-1 (Guadix-Baza basin, Spain). Quat. Int. 389, 191-212.

Despriée, J., Gageonnet, R., Voinchet, P., Bahain, J.-J., Falguères, C., Varache, F., Courcimault, G. and Dolo, J.-M. (2006). Une occupation humaine au Pléistocène inférieur sur la bordure nord du Massif central. Comptes Rendus Palevol 5(6): 821-828.

Despriée, J., Voinchet, P., Bahain, J.-J., Tissoux, H., Falguères, C., Dépont, J., et Dolo, J.-M., 2007. Les nappes alluviales pléistocènes de la vallée moyenne du Cher (région Centre, France): contexte morpho-sédimentaire, Chronologie RPE et Préhistoire. Premiers résultats. Quaternaire 18 (4), 349e368.

Despriée, J., Voinchet, P., Tissoux, H., Moncel, M-H., Arzarello, M., Robin, S., Bahain, J-J., Falguères, C., Courcimault, G., Dépont, J., Gageonnet, R., Marquer, L., Messager, E., Abdessadok, S., Puaud, S. (2010a). Lower and Middle Pleistocene human settlements in the middle Loire River Basin, Centre Region, France. Quaternary International 223-224: 345-359.

Despriée, J., Moncel, M.H., Arzarello, M., Robin, S., Sala, R., Voinchet, P., Gageonnet, R, Bahain, J.J., Falguères, C., Tissoux, H., Dépont, J. et Courcimault, G., (2010b). Lower Pleistocene Sites in the Middle Loire River Basin, Centre region, France, Actes du Congrès international, EarlyPaleolithic of Eurasia: New discoveries, International Conference, Krasnodar-Temriuk, Russie, S.A. Vasil'ev & V.E. Schelinsky (eds.), Académie des Sciences de Russie, Saint-Petersbourg, Centre for Oriental Studies Publishers, Archaeologica Petropolitana, p. 211-225.

Despriée, J., Voinchet, P., Tissoux, H., Bahain, J-J., Falgueres, C., Courcimault, G., Dépont, J., Moncel, M-H., Robin, S., Arzarello, M., Sala, R., Marquer, L., Messager, E., Puaud, S., Abdessadok, S. (2011). Lower and Middle Pleistocene human settlements recorded in fluvial deposits of the middle Loire River Basin, Centre Region, France. Quaternary Science Reviews, 30(11-12): 1474-1485.

Despriée, J., G. Courcimault, M.-H. Moncel, P. Voinchet, H. Tissoux, S. Puaud, X. Gallet, J.-J. Bahain, D. Moreno and C. Falgueres (2016). The Acheulean site of la Noira (Centre region, France): Characterization of materials and alterations, choice of lacustrine millstone and evidence of anthropogenic behaviour. Quaternary International 411: 144-159.

Despriée, J., Courcimault, G., Voinchet, P., Jouanneau, J.C., Puaud, S., Abdessadok, S., Dépont, J., Duval, M., Lebon, M., Ingicco, T., Moncel, M.H., Falguères, C. & Bahain, J.J. (2017a). Le site du pléistocène inférieur de Lunery-Rosières, la Terre-des-Sablons (France, région Centre, Cher): unités sédimentaires, datations ESR, études géoarchéologiques, préhistoire. Quaternaire.

Despriée, J., Voinchet, P., Courcimault, G., Bahain, J.-J., Puaud, S., Moreno, D., Chantreau, Y., Tissoux, H., Gallet, X., Chapon Sao, C., Abdessadok, S. & Falguères, C. (2017b). Le site pléistocène moyen de la Noira à Brinay (Cher, région Centre, France): contexte morphosédimentaire, géochronologie et données archéologiques. Quaternaire, 28(1) : 31-48.

Despriée, J., Courcimault, G., Voinchet, P., Tissoux, H., Bahain, J.-J., Falguères, C. Géochronologie et Préhistoire des nappes fluviatiles fossiles du Loir vendômois à Naveil, Villiers, Thoré et Lunay (Loir-et-Cher) (2017c). Bulletin de la Société Archéologique Scientifique & Littéraire du Vendômois, pp23 – 47.

Duller, G.A.T. Luminescence dating: Guidelines on using luminescence dating in archaeology. English Heritage, Swindon, 2008.

Durcan, J.A., Duller, G.A.T., 2011. The fast ratio: a rapid measure for testing the dominance of the fast component in the initial OSL signal from quartz. Radiat. Meas. 46, 1065-1072.

Durcan, J.A., King, G. E. and Duller, G. A. T. (2015). DRAC: Dose Rate and Age Calculator for trapped charge dating. Quaternary Geochronology 28(0): 54-61.

Duval, M. (2012). Dose response curve of the ESR signal of the Aluminum center in quartz grains extracted from sediment. Ancient TL 30(2): 1-9.

Duval, M. and Guilarte Moreno, V. (2012). Assessing the influence of the cavity temperature on the ESR signal of the Aluminum center in quartz grains extracted from sediment. Ancient TL 30(2): 11-16.

Duval, M. and Arnold, L. J. (2013). Field gamma dose-rate assessment in natural sedimentary contexts using $LaBr_3$(Ce) and NaI(Tl) probes: A comparison between the “threshold” and “windows” techniques. Applied Radiation and Isotopes 74(0): 36-45.

Duval, M. and Guilarte, V. (2015). ESR dosimetry of optically bleached quartz grains extracted from Plio-Quaternary sediment: Evaluating some key aspects of the ESR signals associated to the Ti-centers. Radiation Measurements 78(0): 28-41.

Duval, M., J.-J. Bahain, C. Falguères, J. Garcia, V. Guilarte, R. Grün, K. Martínez, D. Moreno, Q. Shao and P. Voinchet (2015). Revisiting the ESR chronology of the Early Pleistocene hominin occupation at Vallparadís (Barcelona, Spain). Quaternary International 389: 213-223.

Duval, M., Arnold, L. J., Guilarte, V., Demuro, M., Santonja, M. and Pérez-González, A. (2017a). Electron spin resonance dating of optically bleached quartz grains from the Middle Palaeolithic site of Cuesta de la Bajada (Spain) using the multiple centres approach. Quaternary Geochronology 37: 82-96.

Duval, M., Bahain, J.-J., Bartz, M., Falguères, C., Guilarte, V., Moreno, D., Tissoux, H. del Val, M., Voinchet, P. (2017b). Defining minimum requirements for reporting ESR dating methodology and age estimates based on optically bleached quartz grains. Ancient TL 35(1), pp. 11-19.

Fisher, R.A., 1953. Dispersion on a sphere. Proc. Roy. Soc. London, Ser. A, 217: 295-305.

Forman, S. L., Pierson, J. and Lepper, K. (2000). Luminescence Geochronology. Quaternary Geochronology: methods and applications. Sowers, J., Noller, J. and Lettis, W.R. Washington, DC, American Geophysical Union: 157-176.

Galbraith, R.F., Roberts, R.G., Laslett, G.M., Yoshida, H., Olley, J.M., 1999. Optical dating of single and multiple grains of quartz from Jinmium rock shelter, northern Australia: part I, experimental design and statistical models. Archaeometry 41, 339-364.

Garon, H., Voinchet, P., Bahain, J.-J., Despriée, J., Courcimault, G., Tissoux, H., andFalguères, C., Datation ESR de quartz fluviatiles: nouvelles données chronologiques pour le secteur «

intermédiaire » de la vallée de la Creuse (Indre, région Centre, France). Quaternaire, 28(1) : 2017, 73-85.

Grün, R. (1994). A cautionary note: use of 'water content' and 'depth for cosmic ray dose rate' in AGE and DATA programs. Ancient TL 12(2): 50-51.

Guérin, G., Mercier, N. and Adamiec, G. (2011). Dose-rate conversion factors: update. Ancient TL 29(1): 5-8.

Iovita R., Tuvi-Arad I., Moncel M.-H., Despriée J., Voinchet P. and Bahain J.-J. (2017). High Handaxe Symmetry at the beginning of the European Acheulian: The data from la Noira (France) in context. PLOS ONE 12 (5): e0177063.

Kreutzer, S., M. Duval, M. Bartz, P. Bertran, M. Bosq, F. Eynaud, F. Verdin and N. Mercier (2018). Deciphering long-term coastal dynamics using IR-RF and ESR dating: a case study from Médoc, south-west France. Quaternary Geochronology 48: 108-120.

Lisiecki, L. E. and M. E. Raymo (2005). A Pliocene-Pleistocene stack of 57 globally distributed benthic δ18O records. Paleoceanography 20(1): n/a-n/a.

Mejdahl, V., 1979. Thermoluminescence dating: beta-dose attenuation in quartz grains. Archaeometry 21, 61-72.

Méndez-Quintas, E., Santonja, M., Pérez-González, A., Duval, M., Demuro, M. and Arnold, L. J. (2018). First evidence of an extensive Acheulean large cutting tool accumulation in Europe from Porto Maior (Galicia, Spain). Scientific Reports 8(1): 3082.

Moncel, M.H., Despriée, J., Voinchet, P., Tissoux, H., Moreno, D., Bahain, J. J., Courcimault, G., Falgueres, C. (2013). Early evidence of Acheulean settlement in north-western Europe – la Noira site, a 700 000 year-old occupation in the Centre of France. Plos One, 8(11): 1-22.

Moncel, M.-H., et al. (2018). The assemblages with bifacial tools in Eurasia (first part). What is going on in the West? Data on western and southern Europe and the Levant. Comptes Rendus Palevol 17(1): 45-60.

Okada, M., Suganuma, Y., Haneda, Y. and Kazaoka, O. (2017). Paleomagnetic direction and paleointensity variations during the Matuyama–Brunhes polarity transition from a marine succession in the Chiba composite section of the Boso Peninsula, central Japan. Earth, Planets and Space 69(1): 45.

Parés, J.M.; Álvarez, C.; Sier, M.; Moreno, D., Duval, M.; Woodhead, J.D.; Ortega, A.I.; Campaña. I., Rosell, J.; Bermúdez de Castro, J.M.; Carbonell, E., 2018. Chronology of the cave interior sediments at Gran Dolina archaeological site, Atapuerca (Spain). Quat. Sci. Rev., 168:1-16.

Pereira, A., Nomade, S., Moncel, M.-H., Voinchet, P., Bahain, J.-J., Biddittu, I., Falguères, C., Giaccio, B., Manzi, G., Parenti, F., Scardia, G., Scao, V., Sottili, G. and Vietti, A. (2018). Integrated geochronology of Acheulian sites from the southern Latium (central Italy): Insights on human-environment interaction and the technological innovations during the MIS 11-MIS 10 period. Quaternary Science Reviews 187: 112-129.

Prescott, J. R., Hutton, J. T. (1988). Cosmic ray and gamma ray dosimetry for TL and ESR. Nuclear Tracks Radiation Measurements 14: 223-227.

Prescott, J. R., Hutton, J. T. (1994). Cosmic ray contributions to dose rates for luminescence and ESR dating: Large depths and long-term time variations. Radiation Measurements 23: 497-500.

Scott, G. R. and Gibert, L. (2009). The oldest hand-axes in Europe. Nature 461(7260): 82-85.

Shen G., Michel V., Despriée, J., Han F., Granger, D. (2012). Datation d'enfouissement par 26Al/10Be et son application préliminaire à des sites du Paléolithique Inférieur en Chine et en France. L'Anthropologie 116 (1): 1-11.

Tissoux, H., et al. (2007). Potential use of Ti-center in ESR dating of fluvial sediment. Quaternary Geochronology 2(1–4): 367-372.

Tissoux, H, Despriée J, Voinchet P, Bahain JJ, Falguères C, Duvialard J, (2011). Intérêt de la datation par ESE d'un transect complet pour la compréhension d'un système fluviatile : Exemple de la vallée du Loir. Quaternaire, 22, (4), 345-356.

Toro-Moyano, I., Martínez-Navarro, B., Agustí, J., Souday, C., Bermúdez de Castro, J. M., Martinón-Torres, M., Fajardo, B., Duval, M., Falguères, C., Oms, O., Parés, J. M., Anadón. P., Julià, R., García-Aguilar, J. M., Moigne, A.-M., Espigares, M. P., Ros-Montoya, S. and Palmqvist, P. (2013). "The oldest human fossil in Europe, from Orce (Spain)." Journal of Human Evolution 65(1): 1-9.

Toyoda, S., Voinchet, P., Falguères, C., Dolo, J. M. and Laurent, M. (2000). Bleaching of ESR signals by the sunlight: a laboratory experiment for establishing the ESR dating of sediments. Applied Radiation and Isotopes 52(5): 1357-1362.

Toyoda, S., and Falguères, C. (2003). "The method to represent the ESR signal intensity of the aluminium hole center in quartz for the purpose of dating." Advances in ESR Applications 20: 7-10.

Vandenberghe, D., De Corte, F., Buylaert, J. P., Kučera, J. and Van den haute, P. (2008). On the internal radioactivity in quartz. Radiation Measurements 43(2–6): 771-775.

Voinchet, P. (2002). Datation par résonance paramagnétique électronique (RPE) de quartz blanchis extraits de sédiments fluviatiles pléistocènes: contribution méthodologique et application aux systèmes de la Creuse, du Loir et de l'Yonne, thèse, MNHN, Paris, 2002.

Voinchet, P., Falguères, C., Laurent, M., Toyoda, S., Bahain, J.J. and Dolo, J.M. (2003). "Artificial optical bleaching of the Aluminium center in quartz implications to ESR dating of sediments." Quaternary Science Reviews 22(10–13): 1335-1338.

Voinchet, P., Bahain, J.J., Falguères, C., Laurent, M., Despriée, J., Gageonnet, R., Chaussé, C. (2004). "ESR dating of quartz extracted from Quaternary sediments : application to fluvial terraces system of nothern France." Quaternaire 15(1-2): 135-141.

Voinchet, P., Despriée, J., Gageonnet, R., Bahain, J. J., Tissoux, H., Falguères, C., Dépont, J., Dolo, J. M. & Courcimault, G. (2007). Datation par ESR de quartz fluviatiles dans le bassin de la Loire moyenne en région Centre: mise en évidence de l'importance de la tectonique quaternaire et de son influence sur la géométrie des systèmes de terrasses. Quaternaire, 18 (4) 335-347.

Voinchet, P., Despriée, J., Tissoux, H., Falguères, C., Bahain, J. J., Gageonnet, R., Dépont, J. and Dolo, J. M. (2010). ESR chronology of alluvial deposits and first human settlements of the Middle Loire Basin (Region Centre, France). Quaternary Geochronology 5(2–3): 381-384.

Voinchet, P., Yin, G., Falguères, C., Liu, C., Han, F., Sun, X. and Bahain, J. J. (2013). ESR dose response of Al center measured in quartz samples from the Yellow River (China): Implications for the dating of Upper Pleistocene sediment. Geochronometria 40(4): 341-347.

Yokoyama, Y, Falgueres, C., and Quaegebeur, J. P. (1985). ESR dating of quartz from quaternary sediments: First attempt. Nuclear Tracks and Radiation Measurements (1982) 10(4–6): 921-928.

Zijderveld, J.D.A. 1967. AC demagnetization of rocks: Analysis of results. In Collinson, D.W.

Runcorn, S.K. and Creer, K.M. (Eds.), Methods in Paleomagnetism. New York: Elsevier. pp. 254-286.

Table caption

Table 1: ESR data derived from the measurement of the Al centre. Measurement repeatability is expressed as the variation (one relative standard deviation) of the mean ESR intensity obtained from all the aliquots of a given sample after each day of measurement. Similarly, the repeatability of the D_E values corresponds to the variation (one relative standard deviation) of the D_E values calculated for each day of measurement. Bleaching coefficient (%) is defined as the relative difference between the ESR intensities of the natural and bleached aliquots.

Table 2: ESR data derived from the measurement of the Ti centre. Measurement repeatability is expressed as the variation (one relative standard deviation) of the mean ESR intensity obtained from all the aliquots of a given sample after each day of measurement. Similarly, the repeatability of the D_E values corresponds to the variation (one relative standard deviation) of the D_E values calculated for each day of measurement.

Table 3: Detail of ESR age estimates and dose rate components. Errors are 1 sigma.

Table 4: TT-OSL dose rate data, single-grain equivalent doses (D_E) and final ages for samples CRF11-2 and CRF11-4. The final TT-OSL ages have been derived by dividing the weighted mean D_E by the total dose rate.

Table 5: Summary of paleomagnetic data. Dec / Inc: Declination and Inclination of the Characteristic Remanent (ChRM) Magnetization direction; MAD: Maximum angular deviation; Plat / Plong: Latitude and longitude of the Virtual Geomagnetic Pole (VGP) position. Samples LUN1 and NOR1-6 did not yield conclusive (n.c.) results.

Figure caption

Figure 1. A: Geological map of the Centre Region (France) including the middle Loire Basin and junction of the River Loire River and its main tributaries (Loir, Cher and Creuse) (modified from Despriée et al., 2011). The circles indicate the Palaeolithic sites identified in the three valleys. Key: 1 = Lunery-la Terre-des Sablons ; 2 = Brinay-la Noira ; 3= Gievres-la Genetière ; 4 = Gièvres-la Morandière; 5 = Gièvres-la Plaine-de-la-Morandière. B: Synthetic chronostratigraphy of the Cher valley terasse system (Despriée et al., 2011).

Figure 2: Geological context of Lunery-la Terre-des Sablons (LTS) site in the so-called "Les Sablons" block, which is delimited to the west and east by the Rosières fault and Cher river channel, respectively. Local subsidence phenomena have affected the block, which has been successively stripped in various subsets (as indicated by vertical arrows labelled 1, 2 and 3). This interpretation is based on field observations, sedimentological and geochronological evidence collected before the present study, as summarized in section 1.2 and in Despriée et al., (2007a). The position of the archaeological excavation is indicated.

Figure 3: Stratigraphic column of Lunery-la Terre-des Sablons site (modified from Despriée et al., 2007a). The position of all the samples (and their corresponding age results) collected for dating purpose is indicated (Red = ESR sample MNHN; Green = ESR sample CENIEH; Purple = TT-OSL sample; Blue = palaeomagnetic sample; Yellow = TCN sample). TCN and MNHN ESR age results have been previously published in Shen et al. (2012) and Despriée et al., (2007a) (and references therein), respectively. Dose rate and ESR age calculation details may be found in Supplementary Information, Tables S1. Colours are available in the pdf version of the paper.

Figure 4: Stratigraphic column of Brinay-La Noira site (modified from Moncel et al., 2013). The position of all the samples (and their corresponding age results) collected for dating purpose is indicated (Red = ESR sample MNHN; Green = ESR sample CENIEH; Purple = TT-OSL sample; Blue = palaeomagnetic sample; Yellow = TCN sample). Three MNHN ESR samples have not been published elsewhere earlier. The other TCN and MNHN ESR age results have been previously published in Shen et al. (2012) and Despriée et al., (2011), respectively. Dose rate and ESR age calculation details may be found in Supplementary Information, Tables S2. Colours are available in the pdf version of the paper.

Figure 5: Comparison of the ESR ages obtained by MNHN and CENIEH at Lunery-la Terre-des Sablons and Brinay-La Noira sites. Results are grouped per layer. Corresponding numerical

values can be found in Supplementary Information, Tables S1 and S2. Colours are available in the pdf version of the paper.

Figure 6: Sensitivity tests performed on the four CENIEH samples to evaluate the impact of internal dose rate and water content assumptions on the ESR age results derived from the Al centre. Key: black circles = initial age calculation (Fig. 5), with internal dose rate = 50 µGy/a and water content = 20%; red triangles = ESR age results with internal dose rate = 50 µGy/a and water content = 10%; Green squares = ESR age results internal dose rate = 0 µGy/a and water content = 20%. Colours are available in the pdf version of the paper.

Figure 7: Graphical summary of the chronologies obtained in the present work for the fluvial and slope deposits, as well as for the human presence at LTS and BN localities. MIS data are from Lisiecki & Raymo (2005)

Table 1.

Sample	Number of measurement	Bleaching Coefficient (%)	Repeatability of the ESR intensities (%)	Repeatability of the D_E estimates (%)	Adjusted r^2	D_E value (Gy)
LUN1101	3	58.0 ± 1.8	1.8	7.0	0. 993	2560 ± 204
LUN1103	5	55.7 ± 1.6	7.4	12.7	0. 993	2391 ± 129
NOI1101	3	50.7 ± 0.7	1.4	7.3	0.994	1788 ± 113
NOI1104	3	57.4 ± 1.9	3.4	8.6	0.989	2639 ± 256

Table 2.

Option	A		D				E	
Sample ID	Adj. r^2	D_E (Gy)	Measurement repeatability (%)	D_E repeatability (%)	Adj. r^2	D_E (Gy)	Adj. r^2	D_E (Gy)
LUN1101	0.991	2688 ± 117	0.5	8.5	0.987	1934 ± 101	0.993	2802 ± 113
LUN1103	0.987	2143 ± 98	1.1	15.4	0.987	1951 ± 99	0.988	2660 ± 114
NOI1101	0.991	1700 ± 63	1.3	8.6	0.995	1712 ± 93	0.993	2270 ± 50
NOI1104	0.992	2357 ± 113	0.8	16.0	0.986	2074 ± 109	0.994	3078 ± 214

Table 3.

Sample	LUN1101	LUN1103	NOI1101	NOI1104
Unit / Layer	3	1	b	a
Depth (m)	12±3	3.5±0.5	1.5±0.5	7±1
Measured water content (% wet weight)	8.4	7.1	9.8	12.1
Assumed water content (% wet weight)	20±5	20±5	20±5	20±5
Internal dose rate (µGy/a)	50±30	50±30	50±30	50±30
Alpha dose rate (µGy /a)	23±20	28±24	44±39	27±23
Beta dose rate (µGy/a)	2019±177	1639±143	1414±120	1879±162
Gamma dose rate (µGy/a)	821±75	839±77	948±87	781±71
Cosmic dose rate (µGy/a)	44±15	121±11	166±16	72±10
Total dose rate (µGy/a)	2957±238	2677±209	2622±200	2807±221
D_E (Gy) Al centre	2560±212	2391±141	1788±121	2639±263
D_E (Gy) Ti-Li centre	1934±110	1951±108	1712±101	2074±119
Age (ka) Al centre	**866±100**	**893±87**	**682±69**	**940±119**
Age (ka) Ti-Li centre	**654±64**	**729±70**	**653±63**	**739±72**

Table 4

Sample	Site	Layer / Unit	Grain size (µm)	Long-term water content [a]	Environmental dose rate (Gy/ka)				Equivalent dose (D_E) data				TT-OSL age (ka) [f,k]
					Beta dose rate [b,c]	Gamma dose rate [c,d]	Cosmic dose rate [e]	Total dose rate [f,g]	No. of grains [h]	Overdispersion (%) [i]	Age Model [j]	D_E (Gy) [f]	
CRF11-4	BN	*a*	125 – 180	22 ± 4	1.88 ± 0.10	0.85 ± 0.03	0.08 ± 0.01	2.85 ± 0.18	181 / 1900	34 ± 5	CAM	1833 ± 58	644 ± 47
CRF11-2	LTS	3	125 – 180	21 ± 4	2.08 ± 0.11	0.85 ± 0.03	0.05 ± 0.01	3.02 ± 0.18	195 / 2000	29 ± 5	CAM	2194 ± 63	727 ± 51

[a] Long-term water content, calculated as 60% of the present-day saturated water content and expressed as % of dry mass of mineral fraction, with an assigned relative uncertainty of ±20%.

[b] Calculated on dried and powdered sediment samples using a Risø GM-25-5 low-level beta counter.

[c] Specific activities and radionuclide concentrations have been converted to dose rates using the conversion factors given in Guérin *et al.* (2011), making allowance for beta-dose attenuation (Mejdahl, 1979; Brennan, 2003).

[d] Calculated from *in situ* measurements made at each sample position with a NaI:Tl detector, using the 'energy windows' approach (e.g., Arnold *et al.*, 2012b).

[e] Cosmic-ray dose rates were calculated using the approach of Prescott and Hutton (1994), and assigned a relative uncertainty of ±10%.

[f] Mean ± total uncertainty (68% confidence interval), calculated as the quadratic sum of the random and systematic uncertainties.

[g] Includes an internal dose rate of 0.03 Gy/ka with an assigned relative uncertainty of ±30%.

[h] Number of D_E measurements that passed the SAR rejection criteria and were used for D_E determination / total number of grains analysed.

[i] The relative spread in the D_E dataset beyond that associated with the measurement uncertainties for individual D_E values, calculated using the central age model (CAM) of Galbraith *et al.* (1999).

[j] The CAM was used to calculate the final D_E as these samples had overdispersion values consistent with those observed in 'ideal' well-bleached and unmixed sample from similar settings (Arnold and Roberts, 2009; Arnold et al., in press).

[k] Total uncertainty includes a systematic component of ±2% associated with laboratory beta-source calibration.

Table 5.

Specimen	Stratigraphic position	Dec	Inc	MAD	Plat	Plong
Lunery						
LUN2-1A	Unit 1	.8	55.7	5.4	79	179
LUN2-2A	Unit 1	2.1	64.4	2.5	88	120
LUN2-3A	Unit 1	6.7	69.2	10.6	83	36
LUN2-1B	Unit 1	2.6	59.4	7.7	83	166
LUN2-2B	Unit 1	10.4	62.8	4.8	82	109
LUN2-2D	Unit 1	2.5	64.5	12.4	88	112
LUN2-3C	Unit 1	359.0	69.1	7.0	84	356
LUN1	Unit 3	n.c.	n.c.	n.c.	n.c.	n.c.
La Noira						
NOR1-1.1	Layer a (North section)	349.8	47.3	15.8	73	312
NOR1-1.4	Layer a (North section)	7.2	51.1	14.0	70	209
NOR1-2.1	Layer a (North section)	2.8	69.2	20.3	84	18
NOR1-2.3	Layer a (North section)	13.2	59.6	11.9	82	151
NOR1-3.3	Layer a (South section)	17.9	56.7	9.0	82	214
NOR1-3.2	Layer a (South section)	5.2	59.5	7.4	84	237
NOR1-4.1B	Layer a (South section)	354.4	59.2	7.8	81	359
NOR1-4.2C	Layer a (South section)	353.2	62.1	7.5	78	162
NOR1-4.3B	Layer a (South section)	359.1	71.6	15.6	74	159
NOR1-4.1A	Layer a (South section)	.4	59.1	9.6	78	122
NOR1-4.2B	Layer a (South section)	345.2	63.9	11.0	74	122
NOR1-4.3C	Layer a (South section)	349.8	68.2	8.0	83	179
NOR1-5.2	Layer a (South section)	4.9	55.1	12.6	80	269
NOR1-5.4	Layer a (South section)	349.8	47.3	15.8	82	0
NOR1-6	Layer b (North section)	n.c.	n.c.	n.c.	n.c.	n.c.

Figure1

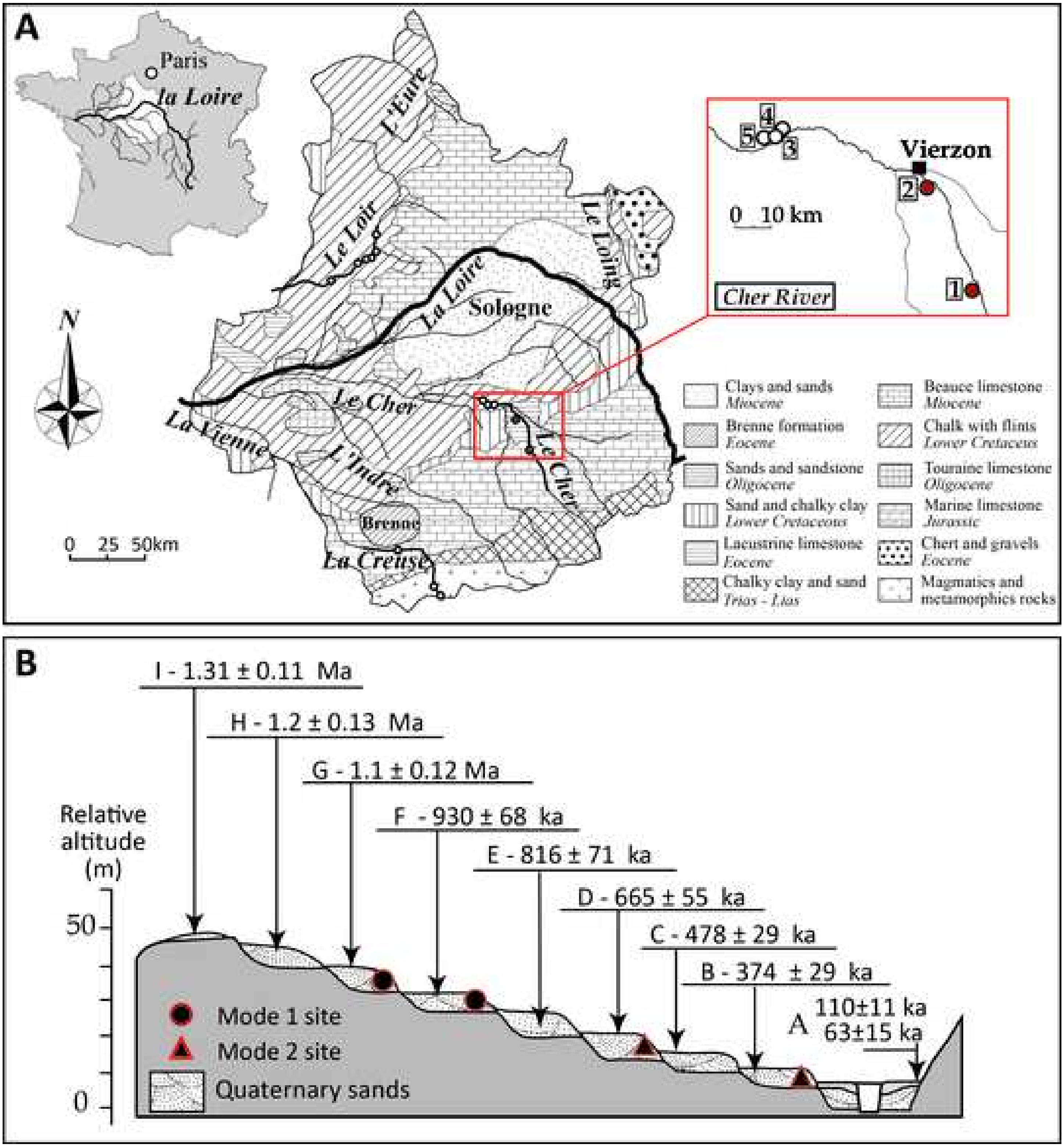
A
Paris
la Loire
N
0 25 50km
L'Eure
Le Loir
Le Loing
La Loire
Sologne
Le Cher
La Vienne
L'Indre
Brenne
La Creuse
Le Cher
4
5
3
Vierzon
2
0 10 km
Cher River
1
Clays and sands
Miocene
Brenne formation
Eocene
Sands and sandstone
Oligocene
Sand and chalky clay
Lower Cretaceous
Lacustrine limestone
Eocene
Chalky clay and sand
Trias - Lias
Beauce limestone
Miocene
Chalk with flints
Lower Cretaceus
Touraine limestone
Oligocene
Marine limestone
Jurassic
Chert and gravels
Eocene
Magmatics and metamorphics rocks
B
I - 1.31 ± 0.11 Ma
H - 1.2 ± 0.13 Ma
G - 1.1 ± 0.12 Ma
F - 930 ± 68 ka
E - 816 ± 71 ka
D - 665 ± 55 ka
C - 478 ± 29 ka
B - 374 ± 29 ka
A
110±11 ka
63±15 ka
Relative altitude (m)
50
0
Mode 1 site
Mode 2 site
Quaternary sands

Figure2

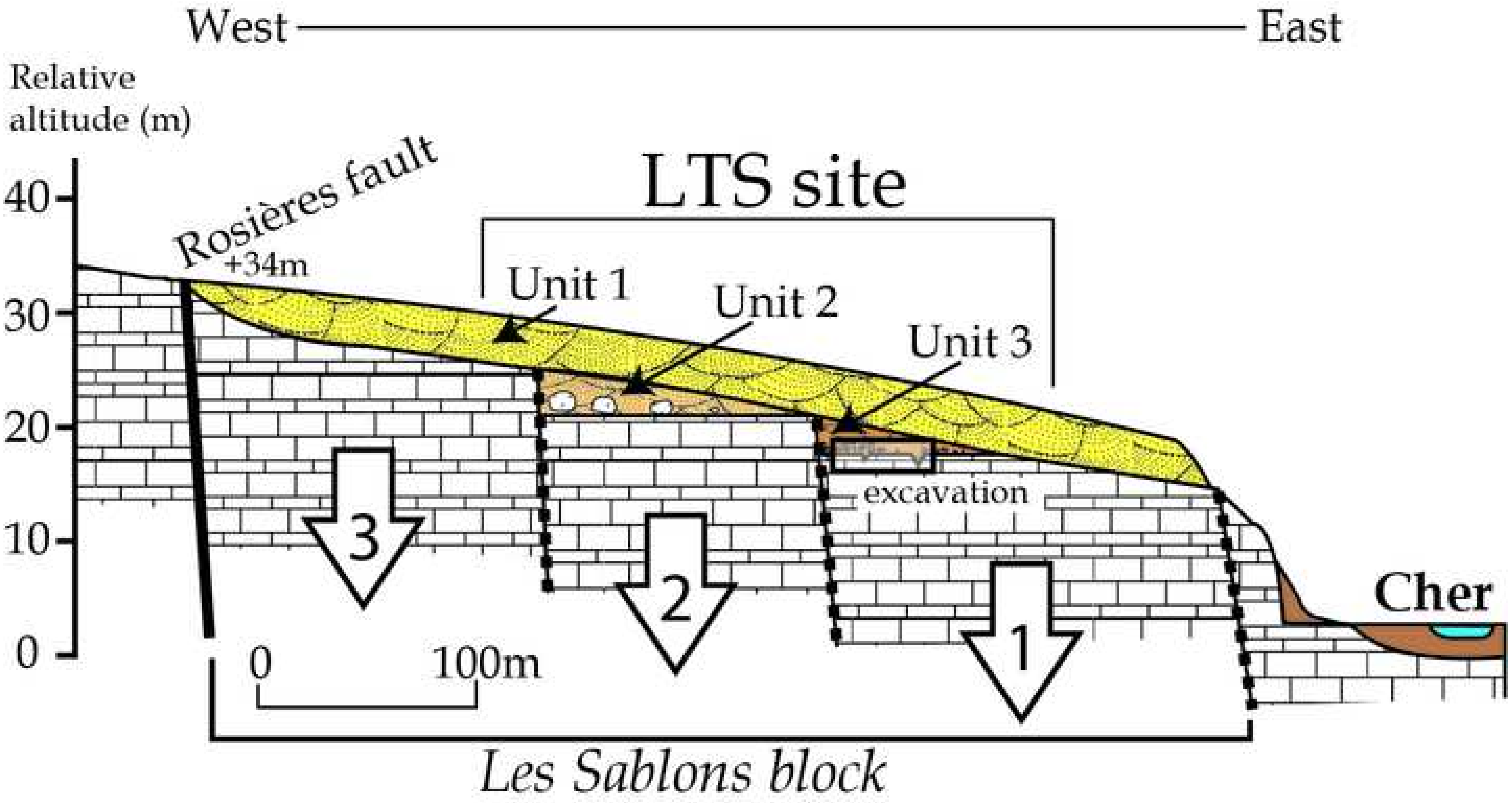
West
East
Relative altitude (m)
40
30
20
10
0
Rosières fault
+34m
LTS site
Unit 1
Unit 2
Unit 3
excavation
3
2
1
0
100m
Cher
Les Sablons block

Figure3

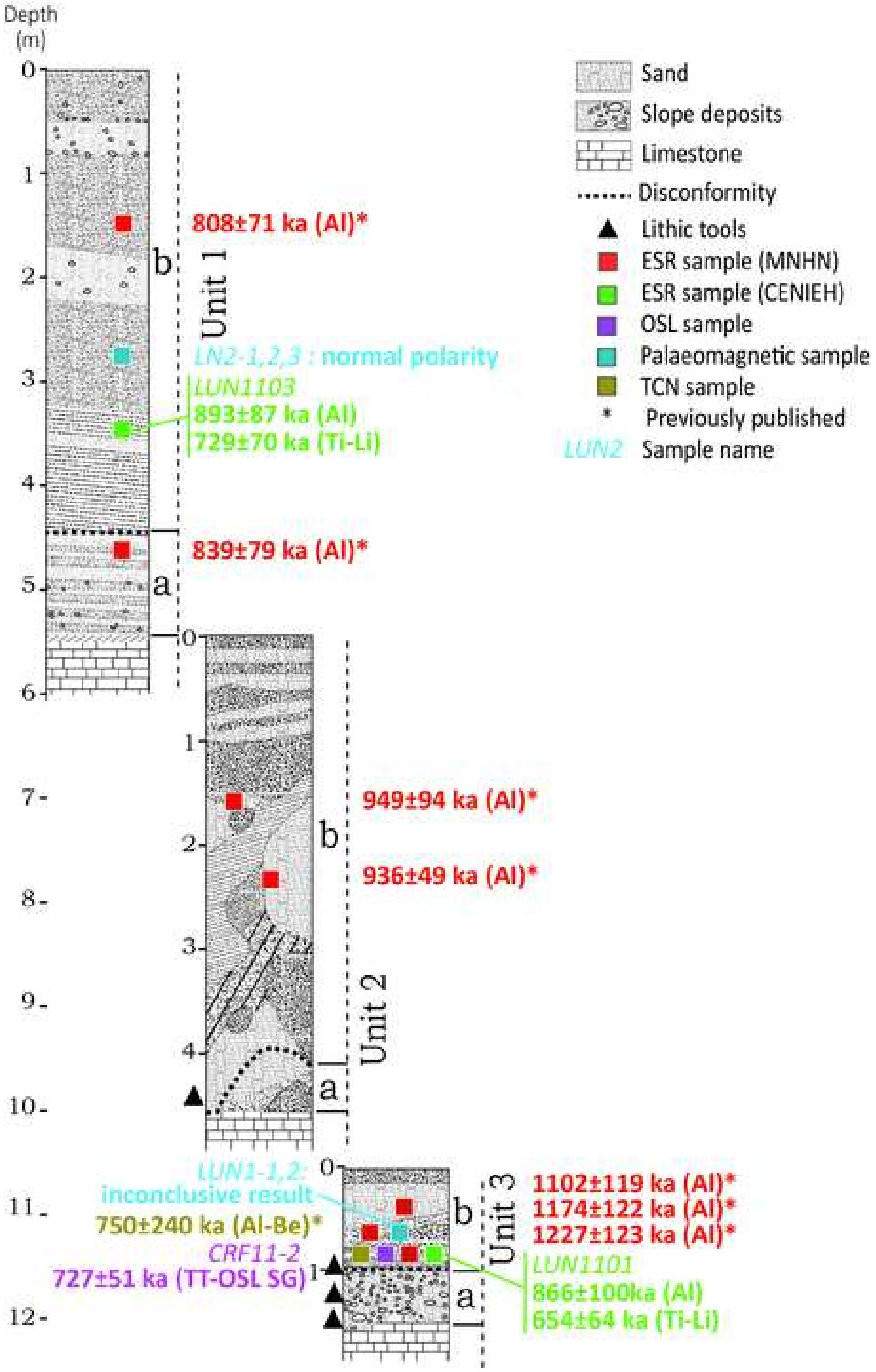
Depth (m)
0
1
2
3
4
5
6
7
8
9
10
11
12
b
a
Unit 1
808±71 ka (Al)*
LN2-1,2,3 : normal polarity
LUN1103
893±87 ka (Al)
729±70 ka (Ti-Li)
839±79 ka (Al)*
0
1
2
3
4
b
a
Unit 2
949±94 ka (Al)*
936±49 ka (Al)*
0
1
b
a
Unit 3
LUN1-1,2:
inconclusive result
750±240 ka (Al-Be)*
CRF11-2
727±51 ka (TT-OSL SG)
1102±119 ka (Al)*
1174±122 ka (Al)*
1227±123 ka (Al)*
LUN1101
866±100ka (Al)
654±64 ka (Ti-Li)
Sand
Slope deposits
Limestone
Disconformity
Lithic tools
ESR sample (MNHN)
ESR sample (CENIEH)
OSL sample
Palaeomagnetic sample
TCN sample
* Previously published
LUN2 Sample name

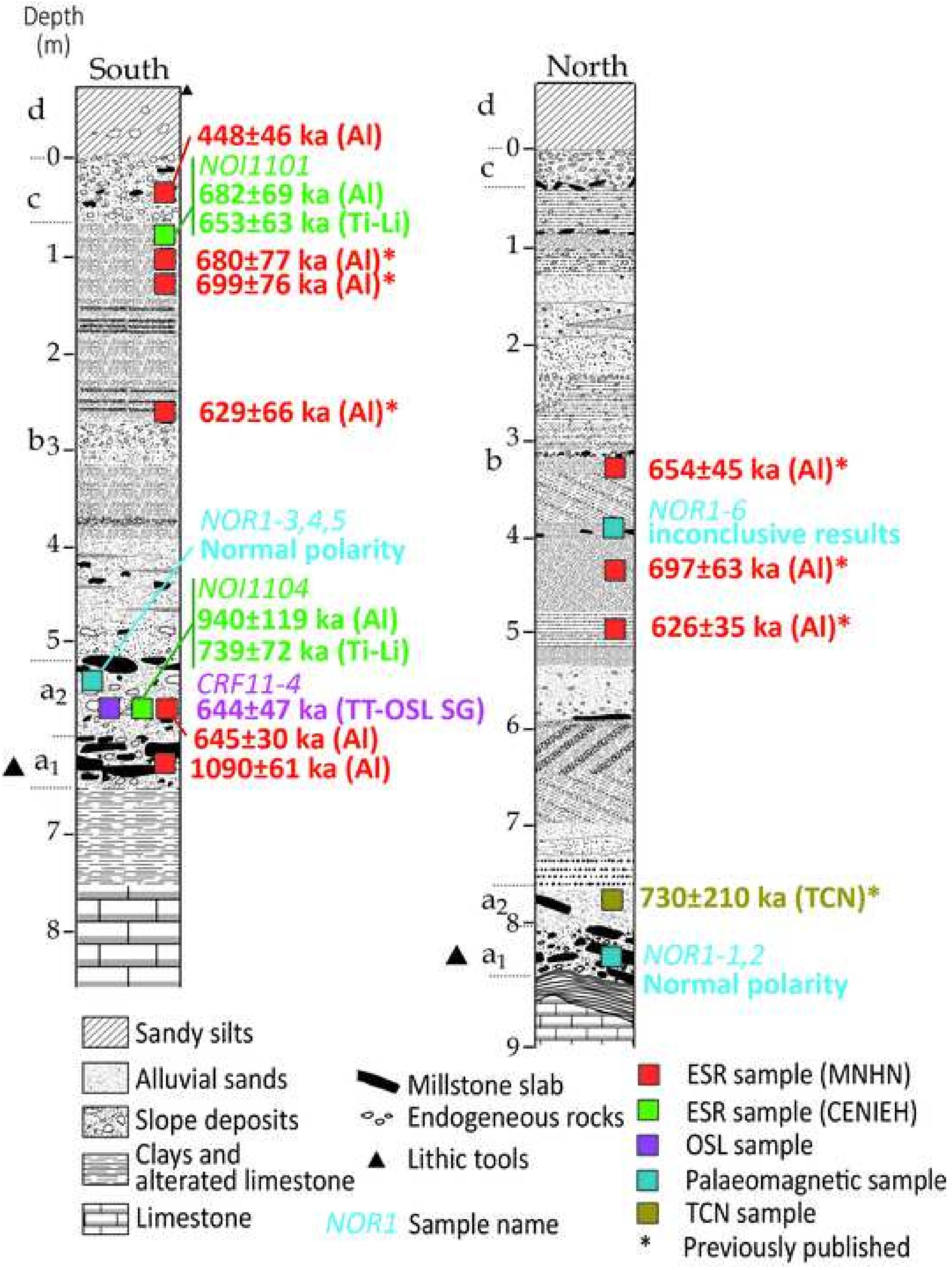
Depth (m)
South
North
d
c
b
b3
a2
a1
0
1
2
3
4
5
6
7
8
9
448±46 ka (Al)
NOI1101
682±69 ka (Al)
653±63 ka (Ti-Li)
680±77 ka (Al)*
699±76 ka (Al)*
629±66 ka (Al)*
NOR1-3,4,5
Normal polarity
NOI1104
940±119 ka (Al)
739±72 ka (Ti-Li)
CRF11-4
644±47 ka (TT-OSL SG)
645±30 ka (Al)
1090±61 ka (Al)
654±45 ka (Al)*
NOR1-6
inconclusive results
697±63 ka (Al)*
626±35 ka (Al)*
730±210 ka (TCN)*
NOR1-1,2
Normal polarity
Sandy silts
Alluvial sands
Slope deposits
Clays and alterated limestone
Limestone
Millstone slab
Endogeneous rocks
▲ Lithic tools
NOR1 Sample name
🟥 ESR sample (MNHN)
🟩 ESR sample (CENIEH)
🟪 OSL sample
Palaeomagnetic sample
TCN sample
* Previously published

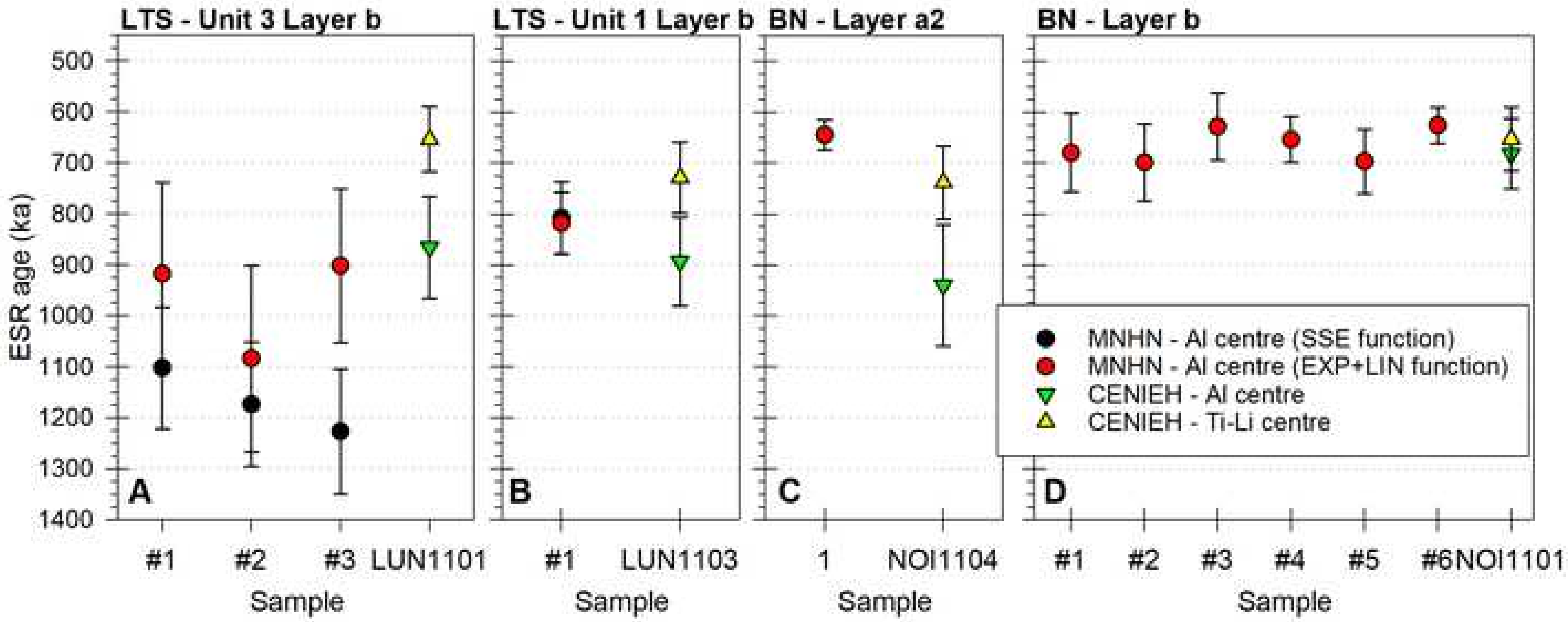
LTS - Unit 3 Layer b
LTS - Unit 1 Layer b
BN - Layer a2
BN - Layer b
ESR age (ka)
500
600
700
800
900
1000
1100
1200
1300
1400
A
B
C
D
#1
#2
#3
LUN1101
#1
LUN1103
1
NOI1104
#1
#2
#3
#4
#5
#6
NOI1101
Sample
Sample
Sample
Sample
● MNHN - Al centre (SSE function)
● MNHN - Al centre (EXP+LIN function)
▼ CENIEH - Al centre
△ CENIEH - Ti-Li centre

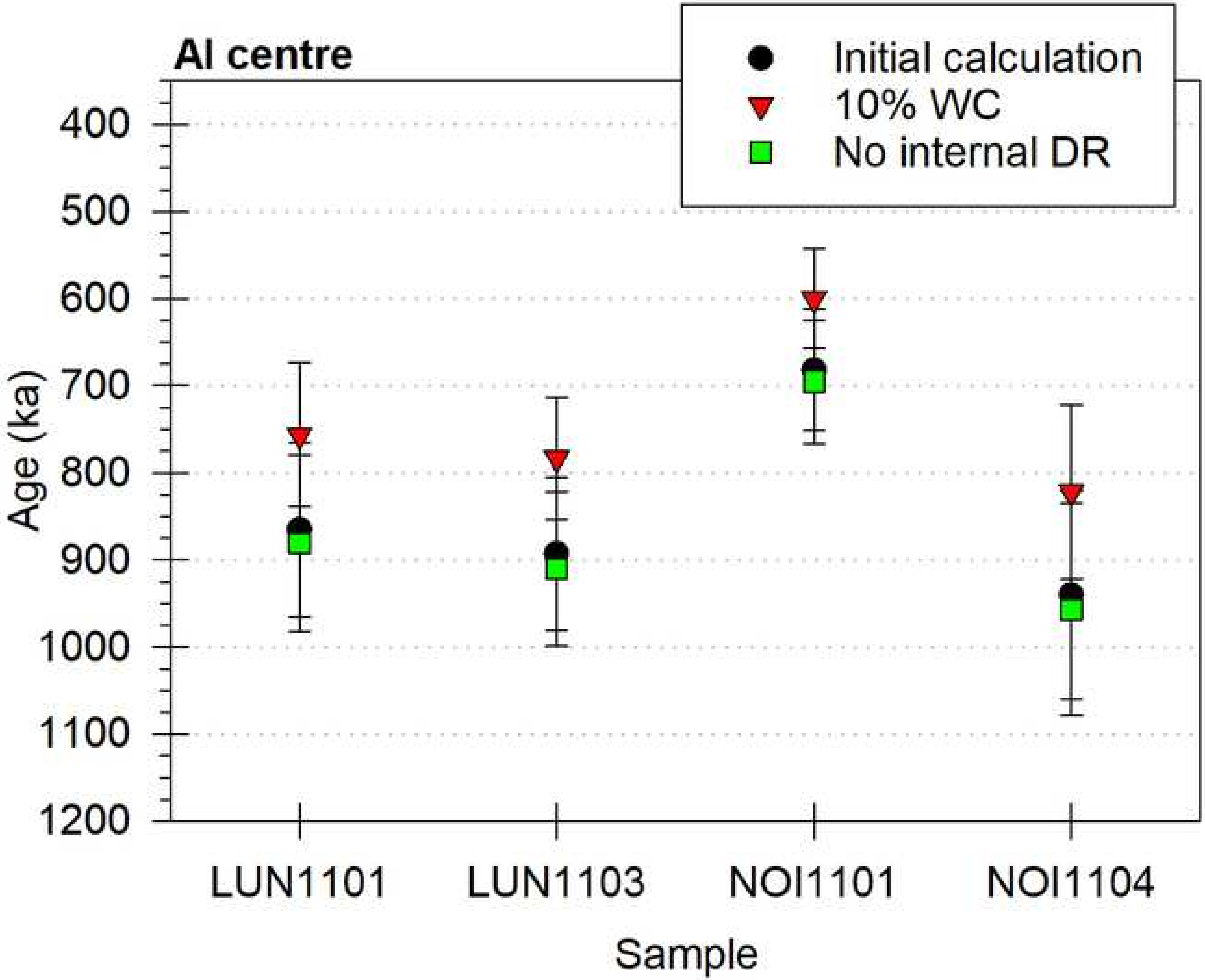
Al centre
● Initial calculation
▼ 10% WC
🟩 No internal DR
Age (ka)
400
500
600
700
800
900
1000
1100
1200
LUN1101
LUN1103
NOI1101
NOI1104
Sample

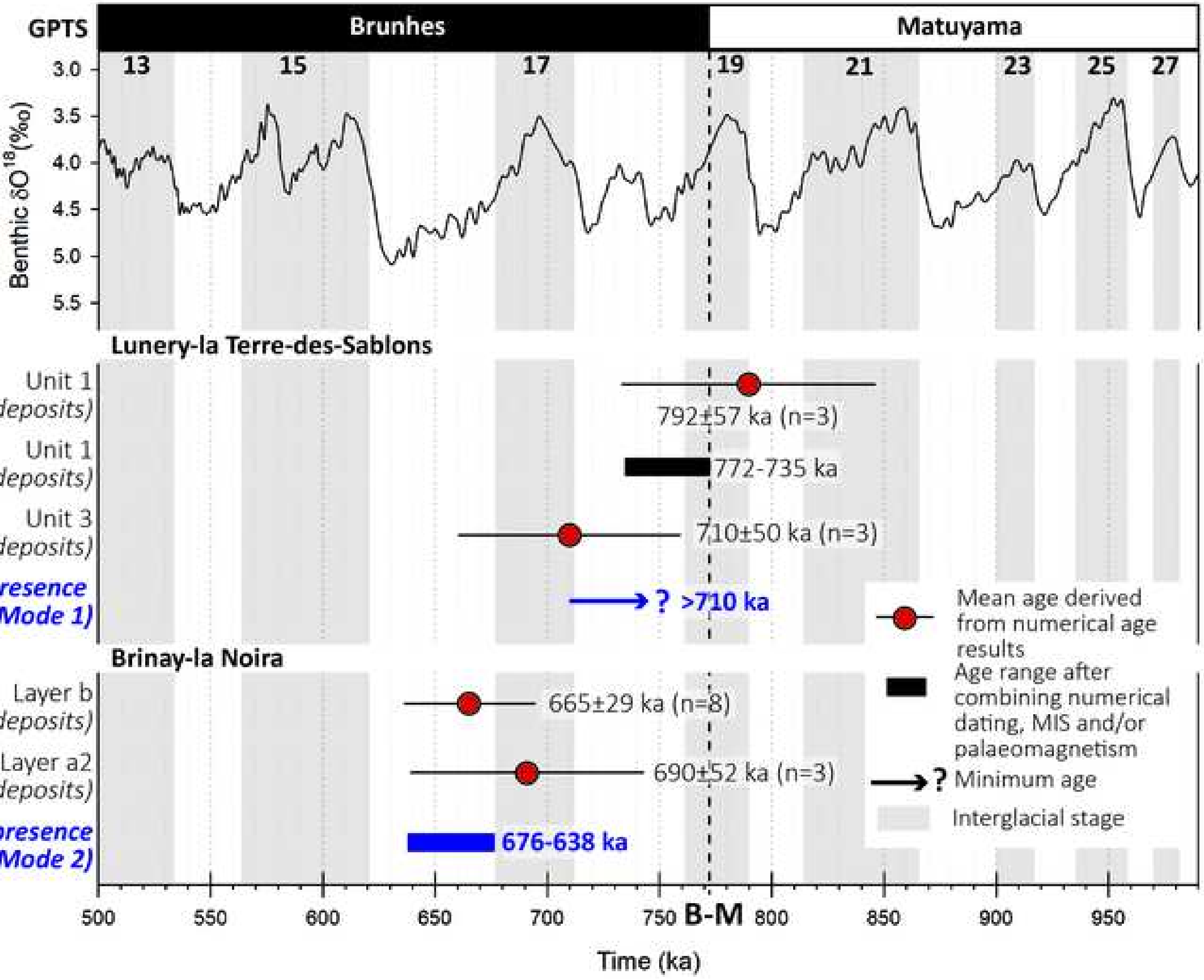
GPTS
Brunhes
Matuyama
13
15
17
19
21
23
25
27
Benthic δO18(‰)
3.0
3.5
4.0
4.5
5.0
5.5
Lunery-la Terre-des-Sablons
Unit 1 (Fluvial deposits)
792±57 ka (n=3)
Unit 1 (Fluvial deposits)
772-735 ka
Unit 3 (Fluvial deposits)
710±50 ka (n=3)
Hominin presence (Mode 1)
? >710 ka
Brinay-la Noira
Layer b (Fluvial deposits)
665±29 ka (n=8)
Layer a2 (Slope deposits)
690±52 ka (n=3)
Hominin presence (Mode 2)
676-638 ka
Mean age derived from numerical age results
Age range after combining numerical dating, MIS and/or palaeomagnetism
? Minimum age
Interglacial stage
500
550
600
650
700
750
B-M
800
850
900
950
Time (ka)